Article

Combination of Coagulation–Flocculation–Decantation and Ozonation Processes for Winery Wastewater Treatment

Nuno Jorge [1,2], Ana R. Teixeira [2], Carlos C. Matos [2], Marco S. Lucas [2] and José A. Peres [2,*]

1   Escuela Internacional de Doctorado (EIDO), Campus da Auga, Campus Universitário de Ourense, Universidade de Vigo, 32004 Ourense, Spain; njorge@uvigo.es
2   Centro de Química de Vila Real (CQVR), Departamento de Química, Universidade de Trás-os-Montes e Alto Douro (UTAD), Quinta de Prados, 5000-801 Vila Real, Portugal; ritamourateixeira@gmail.com (A.R.T.); cmatos@utad.pt (C.C.M.); mlucas@utad.pt (M.S.L.)
*   Correspondence: jperes@utad.pt

Abstract: This research assessed a novel treatment process of winery wastewater, through the application of a chemical-based process aiming to decrease the high organic carbon content, which represents a difficulty for wastewater treatment plants and a public health problem. Firstly, a coagulation–flocculation–decantation process (CFD process) was optimized by a simplex lattice design. Afterwards, the efficiency of a UV-C/ferrous iron/ozone system was assessed for organic carbon removal in winery wastewater. This system was applied alone and in combination with the CFD process (as a pre- and post-treatment). The coagulation–flocculation–decantation process, with a mixture of 0.48 g/L potassium caseinate and 0.52 g/L bentonite at pH 4.0, achieved 98.3, 97.6, and 87.8% removals of turbidity, total suspended solids, and total polyphenols, respectively. For the ozonation process, the required pH and ferrous iron concentration (Fe^{2+}) were crucial variables in treatment optimization. With the application of the best operational conditions (pH = 4.0, $[Fe^{2+}]$ = 1.0 mM), the UV-C/ferrous iron/ozone system achieved 63.2% total organic carbon (TOC) removal and an energy consumption of 1843 kWh·m^{-3}·order^{-1}. The combination of CFD and ozonation processes increased the TOC removal to 66.1 and 65.5%, respectively, for the ozone/ferrous iron/UV-C/CFD and CFD/ozone/ferrous iron/UV-C systems. In addition, the germination index of several seeds was assessed and excellent values (>80%) were observed, which revealed the reduction in phytotoxicity. In conclusion, the combination of CFD and UV-C/ferrous iron/ozone processes is efficient for WW treatment.

Keywords: coagulation–flocculation–decantation; germination index; ozone; potassium caseinate; UV-C radiation; winery wastewater

1. Introduction

Portugal is a Mediterranean wine producer, with an approximated vineyard area of 191,000 ha and a wine production value of 6.4 MhL, in 2020 [1]. This extensive wine production requires large amounts of water, to perform several activities that are necessary to ensure the quality of the wines, such as the floor and equipment washing, rinsing of the transfer lines, barrel cleaning, bottling facilities, filtration units, etc. [2–4]. The high consumption of water inevitably leads to the generation of large amounts of winery wastewaters (WW). The environmental impact of wastewater from the wine industry is highly detrimental if it is released without proper treatment, causing water pollution, soil degradation, and damage to the vegetation by odors and gaseous emissions [2,5]. Currently, the most widespread decontamination approaches are activated sludge reactors [6]; however, the seasonal character of these wastewaters makes it difficult for the microorganisms to adapt. In addition, during the vintage stage, the pollutant loads and wastewater volumes that are produced are higher, requiring longer retention times in the activated sludge reactors, which makes these biologic reactors oversized for most of the year [7].

The coagulation–flocculation–decantation process (CFD process) is one of the most mature and effective processes involved in wastewater treatment, which can remove the suspended particles and most of the colloid particles, by the formation of flocs. Generally, the CFD mechanisms can be categorized into the following four kinds: (1) simple charge neutralization, (2) charge patching, (3) bridging, and (4) sweeping [8,9]. The application of inorganic salt coagulants, such as iron and aluminum, has been reported in the treatment of winery wastewater [10], mature landfill leachate [11], cork processing wastewaters [12], among others. Nonetheless, there are several drawbacks that are associated with the use of these metallic salts, for instance, their high sensitivity to pH, their ineffectiveness on miniscule particles in low temperatures, and the production of large amounts of sludge containing metal hydroxides [13]. In this work, the application of a mixture of potassium caseinate, activated sodium bentonite, and polyvinylpolypyrrolidone was tested, as an alternative to metallic coagulants, which, to the best of our knowledge, have not been applied to the treatment of winery wastewater.

Another alternative to biologic treatments are advanced oxidation processes (AOPs), which are based on the production of hydroxyl radicals ($HO^\bullet$) and are capable of promoting, in a non-selective manner, both the degradation and mineralization of pollutants into CO_2, H_2O, and inorganic salts [14,15]. Among the different AOPs, the following have been reported to be used in the treatment of winery wastewater: the application of the homogeneous Fenton process [16], homogeneous photo-Fenton process [17,18], sulfate radicals [19,20], heterogeneous photo-Fenton process [21,22], and ozonation process [23]. In this work, the application of ozonation, as a complement to the CFD process in the treatment of winery wastewater, was studied. Ozone is an unstable gas, with a characteristically penetrating odor and partial solubility in water. In wastewater treatment, the advantages of ozone are evident, since it is a powerful oxidant, with a redox potential of 2.07 V in alkaline solution, making it able to oxidize several inorganic and organic substances, when compared to other oxidizing agents, such as H_2O_2 (1.77 V), $HO_2^\bullet$ (1.70 V), Cl_2 (1.09 V), and O_2 (0.40 V) [24]. In addition, generated H_2O_2 can considerably enhance the $HO^\bullet$ formation from O_3 decomposition, during the O_3/UV process when compared to conventional ozonation [25,26]. It was observed by several authors that ozone, in combination with UV-C radiation, was effective in the treatment of wastewater with a high polyphenol content, such as that found in the cork manufacturing industry [27], the olive oil industry [28], and the wine distillery industry [29]. In this work, the application of the system O_3/Fe^{2+}/UV-C was tested, which, to our knowledge, has not been hitherto performed in winery wastewater treatment and, therefore, its effects in organic carbon reduction are still unknown.

In order to answer these important questions, the aim of this work is (1) to perform the treatment of winery wastewater using CFD, with the application of potassium caseinate, activated sodium bentonite, and PVPP; (2) to optimize the coagulant mixture by the performance of a simplex lattice design; (3) to optimize the ozonation process; (4) to evaluate the efficiency of the combined CFD/ozonation processes; and, finally, (5) to study the effect of the combined CFD/ozonation processes in the phytotoxicity reduction in plant seeds, and changes in the phenolic and chromatic characteristics of the wastewater.

2. Materials and Methods

2.1. Reagents and Winery Wastewater Sampling

Winery wastewater was collected from a cellar located in the Douro region (Northern Portugal). This agroindustry is a private company dedicated to the production of table wine. It is responsible for receiving grapes and for their processing, from crushing, must fermentation, wine stabilization and filtration, and finally bottling. After collecting the samples in plastic containers to be transported to the laboratory, they were stored at −40 °C. This work was performed at the University of Trás-os-Montes and Alto Douro, located in Vila Real, Portugal, latitude 41°17′9.18″ N and longitude 7°44′21.45″ W.

Activated sodium bentonite was purchased from Angelo Coimbra & Ca., Lda, Maia, Portugal, potassium caseinate and polyvinylpolypyrrolidone (PVPP) from A. Freitas Vi-

lar, Lisboa, Portugal, and ferrous sulphate heptahydrate ($FeSO_4 \bullet 7H_2O$) from Panreac, Barcelona, Spain. NaOH and H_2SO_4 (95%) were both obtained from Analar Normapur, Vila Nova de Gaia, Portugal. Deionized water was used to prepare the respective solutions.

2.2. Analytical Techniques

Different physical–chemical parameters were monitored in order to characterize the WW, including the chemical oxygen demand (COD), the biochemical oxygen demand (BOD_5), the total organic carbon (TOC) and the total polyphenols. The main chemical parameters measured are shown in Table 1. The COD and BOD_5 were determined according to Standard Methods (5220D; 5210D; respectively) [30]. COD analysis was carried out in a COD reactor from HACH Co. (Loveland, CO, USA), and a HACH DR 2400 spectrophotometer (Loveland, CO, USA) was used for colorimetric measurement. Biochemical oxygen demand (BOD_5) was determined using a respirometric OxiTop system. The turbidity was determined by a 2100N IS turbidimeter (Hach, Loveland, CO, USA), pH by a 3510 pH meter (Jenway, Cole-Parmer, UK) and conductivity by a portable condutivimeter, VWR C030 (VWR, V. Nova de Gaia, Portugal). These measurements were determined in accordance to the methodology of the Standard Methods [30]. The TOC content (mg C/L) was determined using a Shimadzu TOC-L CSH analyzer (Shimadzu, Kyoto, Japan). Total polyphenols were evaluated following the Folin–Ciocalteu method [31]. Dissolved ozone was measured by application of the AccuVac Ampul procedure (Ozone AccuVac® Ampules, 0–1.5 mg/L, HACH, Loveland, CO, USA). The ferrous iron concentrations was analyzed by atomic absorption spectroscopy (AAS) using a Thermo Scientific iCE 3000 SERIES (Thermo Fisher Scientific, Waltham, MA, USA).

Table 1. Winery wastewater characteristics.

Parameter	Value
pH	4.0
Conductivity (µS/cm)	475
Turbidity (NTU)	1040
Total suspended solids (mg/L)	2430
Chemical oxygen demand (mg O_2/L)	9432
Biochemical oxygen demand (mg O_2/L)	2611
Total organic carbon (mg C/L)	1962
Total polyphenols (mg gallic acid/L)	123
Ferrous iron (mg Fe/L)	0.05
Biodegradability index—BOD_5/COD	0.28

Phytotoxicity tests were performed by germination of onion, cucumber, lettuce and corn seeds (standard species recommended by the US Environmental Protection Agency, the US Food and Drug Administration, and the Organization for Economic Cooperation and Development [32]) and determined by Equation (1) in accordance to Varnero et al. [33] and Tiquia et Tam [34], as follows:

$$GI(\%) = \frac{\overline{N}_{SG,T}}{\overline{N}_{SG,B}} * \frac{\overline{L}_{R,T}}{\overline{L}_{R,B}} * 100 \qquad (1)$$

where GI is the germination index, $\overline{N}_{SG,T}$ is the arithmetic mean of the number of germinated seeds in each extract (wastewater), $\overline{N}_{SG,B}$ is the arithmetic mean of the number of germinated seeds on standard solution (distilled water), $\overline{L}_{R,T}$ is the mean root length in each extract (wastewater) and $\overline{L}_{R,B}$ is the mean root length in control (distilled water).

Let Xi be defined as the removal of a given indicator (%) of water contamination (turbidity, TSS, TOC, COD and total polyphenols) that is achieved by a treatment (Equation (2)) [12], as follows:

$$X_i(\%) = \frac{C_0 - C_f}{C_0} * 100 \qquad (2)$$

where C_0 and C_f are the initial and final concentrations, respectively, of parameter i.

2.3. Phenolic and Chromatic (CIELab) Characterization

Color intensity (CI) and hue were determined by the OIV method [35], total polyphenol index (TPI) was determined by Curvelo-Garcia method [36], total phenols, non-flavonoids and flavonoids were determined according to Kramling and Singleton [37]. Total anthocyanins were analyzed by SO_2 bleaching method, described by Ribéreau-Gayon et al., [38], colored anthocyanins (*CA*), total pigments (*TP*) and polymeric pigments (*PP*) were analyzed by the method described by Somers and Evans [39], and total tannins were determined by the LA method [40]. All samples were analyzed by a spectrophotometer (GENESYS^{TM} 10 series spectrophotometers). The absorption spectra of WW samples were recorded with a Shimadzu UV-2101 spectrophotometer (Shimadzu, Kyoto, Japan) scanned from a range between 380 and 770 nm, with 5 nm distance, using 1 cm path length quartz cells. Data were collected to determine *L* (lightness), *a* (redness), and *b* (yellowness) coordinates using the CIELab 1976 method. This allows reliable quantification of the overall color difference of a sample when compared to a reference sample (blank). Color differences can be distinguished by the human eye when the differences between ΔE_{ab}^* values are greater than two units, in accordance to Spagna et al. [41]. All analyses were performed in duplicate. Table 2 resumes the formulas used in this work.

Table 2. Formulas for phenolic composition and chromatic (CIELab) determination.

Formulas	Parameters	References
Color intensity (CI) CI = A_{420} + A_{520} + A_{620}	A_{420}—absorbance at 420 nm A_{520}—absorbance at 520 nm	OIV, [35]
Hue Hue = $\frac{A_{420}}{A_{520}}$	A_{620}—absorbance at 620 nm A_{280}—absorbance at 280 nm	OIV, [35]
Total polyphenol index (TPI) TPI = A_{280}*DF	DF—dilution factor	Curvelo-Garcia, [36]
Total phenols Total phenols (mg gallic acid/L) = $\frac{A_{280}^{IPT}+0.0243}{0.0326}$*DF		Kramling and Singleton, [37]
Non-flavonoids Non − flavonoids (mg gallic acid/L) = $\frac{A_{280}^{NF}+0.0243}{0.0326}$*DF		Kramling and Singleton, [37]
Flavonoids Flavonoids (mg gallic acid/L) = total phenols–non-flavonoids		Kramling and Singleton, [37]
Total anthocyanins (C) C (mg/L) = 875*(A_1–A_2)	A_1/A_2—absorbance at 520 nm	Ribéreau-Gayon et al. [38]
Colored anthocyanins (CA) CA (mg/L) = $\left(A_{520}^{no\ bisulfite}*10\right)$–$\left(A_{520}^{bisulfite}*10\right)$		Somers and Evans [39]
Total pigments (TP) TP (mg/L) = A_{520}^{HCl}*10		Somers and Evans [39]
Polymeric pigments (PP) PP (mg/L) = A_{520}^{HCl}*10		Somers and Evans [39]
Total tannins (L.A.) L.A. (g/L) = 19.33*(D_2–D_1)	D_1/D_2—absorbance at 520 nm	Ribéreau-Gayon and Stonestreet [40]
CIELab $\Delta L = L_1 - L_0$ $\Delta a = a_1 - a_0$ $\Delta b = b_1 - b_0$ $\Delta E_{ab} = [(\Delta L)^2 + (\Delta a)^2 + (\Delta b)^2]$	*L*—lightness *a*—redness *b*—yellowness	Schanda [42]

2.4. Coagulants Characterization

The FTIR spectra were obtained by mixing 2 mg of coagulants with 200 mg KBr. The powder mixtures were then inserted into molds and pressed at 10 ton/cm^2 to obtain the transparent pellets. The samples were analyzed with a Bruker Tensor 27 spectrometer and the infrared spectra in transmission mode was recorded in the 4000–400 cm^{-1} frequency region. The microstructural characterization was carried out with a scanning electron microscop (FEI QUANTA 400 SEM/ESEM, Fei Quanta, Hillsboro, WA, USA) and the chemical composition of the different catalysts was estimated (Table 3) using the energy-dispersive X-ray spectroscopy (EDS/EDAX, PAN'alytical X'Pert PRO, Davis, CA, USA).

Table 3. Chemical composition of activated sodium bentonite by EDS/EDAX.

Element	Mass Concentration (wt %)
Si	69.49
Al	17.67
Fe	2.95
Mg	2.73
Ca	2.00
Na	2.76
K	1.37
S	1.03

The textural parameters of samples were obtained from N$_2$ adsorption–desorption isotherms at 77 K using a Micromeritics ASAP 2020 apparatus (TriStar II Plus, Micromeritics Instrument Corporation, Norcross, GA, USA). The samples were degassed at 150 °C up to 10^{-4} Torr before analysis. The specific surface area (SBET) was determined by applying the Gurevitsch's rule at a relative pressure p/p$_0$ = 0.30 and according to the Brunauer, Emmet, Teller (BET) method from the linear part of the nitrogen adsorption isotherms. Different pore volumes were determined by the Barrett, Joyner, Halenda model (BJH model).

From FTIR analysis (Figure 1), potassium caseinate shows a sharp peak at hydrophilic O–H stretching at 3523 cm^{-1} and a strong vibration of hydrophobic C–H stretching (proteins) at 2962 cm^{-1}. Further, a –C=O stretching vibration (amide I) was observed at 1643 cm^{-1}, C–N stretching and N–H bending at 1531 cm^{-1} (characteristic amide II band), a C–H bending deformation and –CH$_3$ symmetrical deformation at 1446 and 1386 cm^{-1}, respectively, and –C–NH$_2$ stretching (amide III) at 1240 cm^{-1} [43,44].

PVPP shows an O–H stretching assigned to the stretching vibration of hydroxyl group (OH) at 3481 cm^{-1} [45], CH$_2$ asymmetric stretching vibration (ring) at 2956 cm^{-1} [46], C–H stretching at 2895 cm^{-1} [45], C=O stretching of PVPP at 1651 cm^{-1} [47–50], CH$_2$ scissoring vibrations at 1463 cm^{-1} [46], C–N stretching or C–O stretching at 1288 cm^{-1} [51], twisting of CH$_2$ of PVPP at 1228 cm^{-1} and CH$_2$ rocking at 1020 cm^{-1} [45,46].

The activated sodium bentonite shows the stretching vibration of structural O–H groups at 3645 cm^{-1}, structural Si–O groups at 1103, 999 and 789 cm^{-1}, structural Al–Al–OH groups at 902 cm^{-1}, structural Al–Fe–OH groups at 883 cm^{-1}, the free and interlayer water in bond stretching vibration at 3396 cm^{-1}, and adsorbed water-yielded bending at 1643 cm^{-1} [52–55].

The results obtained by BET analysis (Table 4) showed that bentonite exhibited a mesoporous structure with a specific surface area of 8.8 m^2/g, a total pore volume of 0.045 cm^3/g and a particle size of 4.0 nm. The respective isotherms can be classified as type II, where unrestricted monolayer–multilayer adsorption occurs, and the behavior of the hysteresis loops can be associated with type H3, which usually corresponds to aggregates of plate-like particles forming slit-like pores [56], which is in agreement with these material structures. Potassium caseinate had a specific surface area of 1.0 m^2/g, PVPP's surface area was not quantifiable. Total pore volume and particle size were not quantifiable for potassium caseinate and PVPP, which indicates that these coagulants have a microporous structure. The shape of its N$_2$ adsorption–desorption isotherm was a type I isotherm,

typical of microporous solids with relatively small external surfaces, as defined by the International Union of Pure and Applied Chemistry (IUPAC) [57].
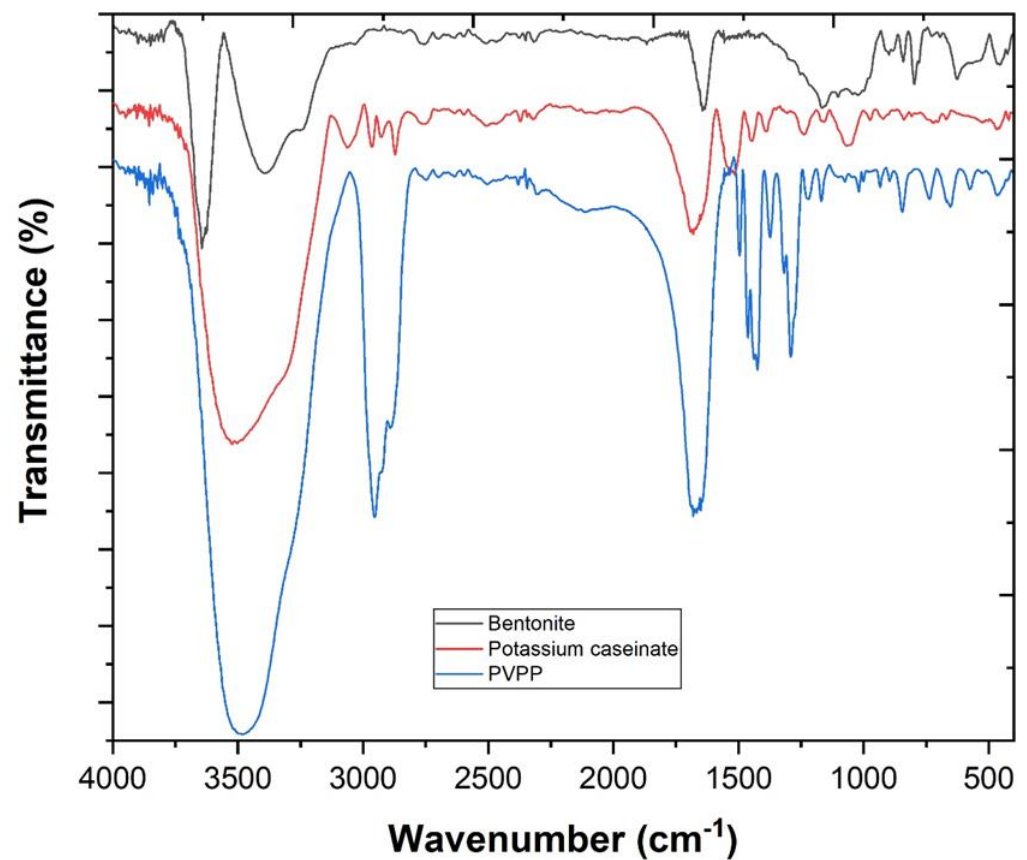

Figure 1. FTIR spectra of bentonite, potassium caseinate and PVPP.

Table 4. Specific surface areas and pore characteristics of coagulants (n.q.—not quantifiable).

Coagulants	S_{BET} (m^2/g)	$V_{total\ pore}$ (cm^3/g)	Particle Size (nm)
Activated sodium bentonite	8.8	0.045	4.0
Potassium caseinate	1.0	n.q.	n.q.
PVPP	n.q.	n.q.	n.q.

2.5. Coagulation–Flocculatuion–Decantation Experiments

CFD experiments were performed in a jar-test apparatus (ISCO JF-4). Several trials were performed using 500 mL of effluent in 1000 mL beakers. Fixed conditions were set as the following: pH 4.0, rapid mixing 150 rpm/3 min, slow mixing 20 rpm/20 min, temperature 298 K, sedimentation period 12 h. The CFD experiments were developed with the statistical software Minitab 18.0 (State College, Pennsylvania, USA), and applied the simplex lattice design (SLD) as follows:

1. Application of bentonite, potassium caseinate and PVPP with a lower and upper dosage of 0 and 1.0 g/L, respectively;
2. Application of maximum mixture dosage of 1.0 g/L.

All the experiments were performed in triplicate and the observed standard deviation was always less than 5% of the reported values. Statistical analysis was performed by OriginLab 2019 software (Northampton, MA, USA).

2.6. Ozonation Experiments

Batch experiments for the ozonation process were performed using an air pump IDEA-R AP2 (1.8 W/1000 ccO_2/min) from SICCE. Oxygen was converted into ozone by an ozone generator 1KNT-24 (25 W) of 1000BT-12 with low working noise (<30 DB). This ozone generator uses high-output corona discharge ozone tube, together with a high Óow ball bearing cooling fan (48 CFM) to ensure steady ozone output (up to 300 mg/hr). Figure 2 shows the setup of the ozone reactor used in this work.
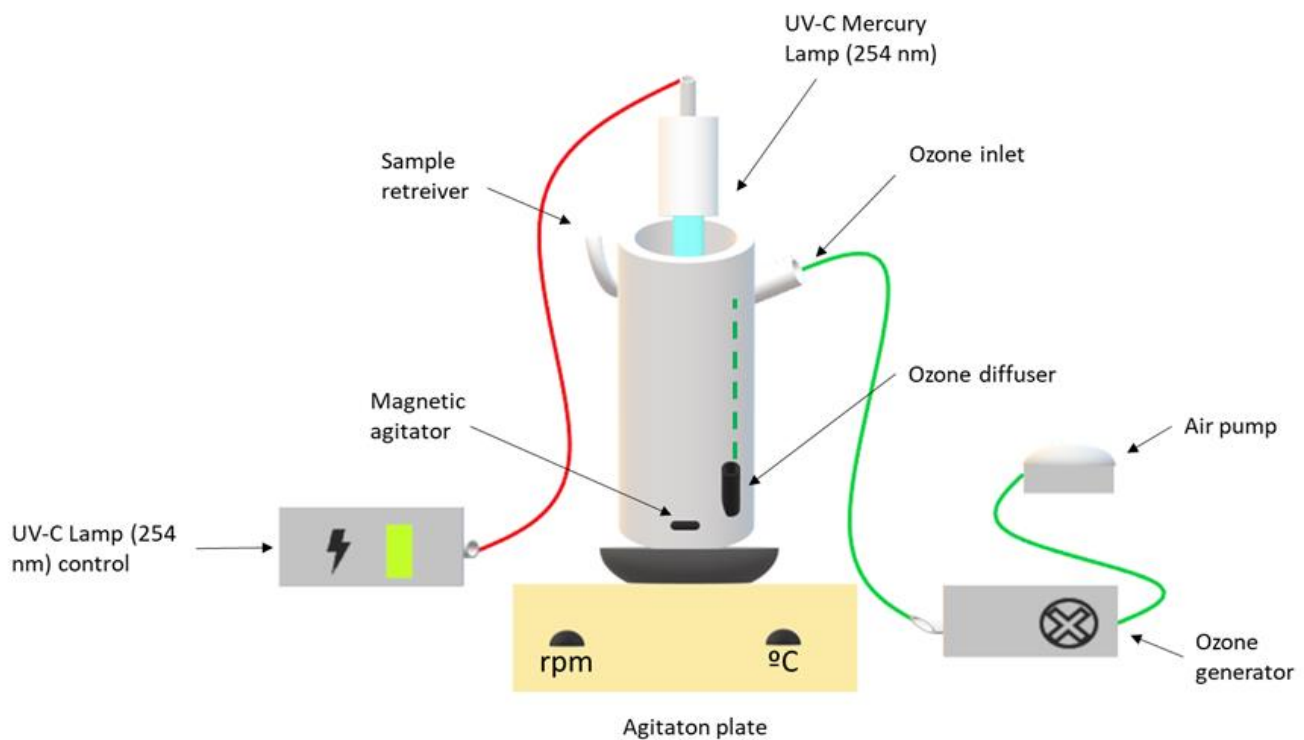

Figure 2. Schematic representation of ozonation and UV reactor.

The photoreactor was fitted with a Heraeus TNN 15/32 lamp (14.5 cm in length and 2.5 cm in diameter), mounted in the axial position inside the reactor. The spectral output of the low-pressure mercury vapor lamp emitted mainly (85–90%) at 253.7 nm and about 7–10% at 184.9 nm. The experiments were carried out as follows:

1. Performance of different pH conditions (4.0, 7.0, 9.0 and 11.0) under the following operational conditions: $[Fe^{2+}]$ = 1.0 mM, ozone flow rate 5 mg/min, air flow 1.0 L/min, agitation 350 rpm and UV-C mercury lamp (254 nm);
2. Performance of different Fe^{2+} concentrations (0.0, 0.5, 1.0 and 2.0) at pH 4.0, ozone flow rate 5 mg/min, air flow 1.0 L/min, agitation 350 rpm and a UV-C mercury lamp (254 nm).

All the experiments were performed in triplicate and the observed standard deviation was always less than 5% of the reported values. Statistical analysis was performed with OriginLab 2019 software (Northampton, MA, USA).

3. Results and Discussion

3.1. Coagulation–Flocculation–Decantation Experiments

3.1.1. Simplex Lattice Design—Model Establishment

In Table 1, it is observed that the WW has high levels of turbidity (1040 NTU), total suspended solids (TSS) (2430 mg/L), and organic content (1962 mg C/L). The CFD process is essential to reduce these parameters, to improve the ozonation treatment efficiency, since the presence of refractory compounds is considered to be hydroxyl radical scavengers. In

addition, without suspended solids, light can better penetrate through the solution, to trigger ozone decomposition [11]. The CFD experiments were performed by a simplex lattice design (SLD), in which seven different tests were performed, to optimize the combination of coagulants. The experimental and predicted values obtained after the assessment of turbidity, TSS, chemical oxygen demand (COD), and total organic carbon (TOC), are listed in Table 5.

Table 5. Design matrix with the experimental and predicted removal percentages of turbidity, TSS, COD and TOC. Experimental conditions: pH 4, temperature 298 K, rapid mix 150 rpm/3 min, slow mix 20 rpm/20 min, sedimentation time 12 h. X_1—potassium caseinate, X_2—bentonite, X_3—PVPP.

Experiments	Samples			Y_1: Turbidity		Y_2: TSS		Y_3: COD		Y_4: TOC	
	X_1	X_2	X_3	Observed	Predicted	Observed	Predicted	Observed	Predicted	Observed	Predicted
CFD1	0.00	1.00	0.00	99.6	99.6	98.3	98.3	54.3	54.4	28.4	28.4
CFD2	0.67	0.17	0.17	99.5	99.5	98.0	98.0	52.9	52.5	32.5	32.4
CFD3	1.00	0.00	0.00	99.5	99.5	97.9	97.9	48.5	48.6	31.6	31.6
CFD4	0.17	0.17	0.67	99.3	99.3	97.9	97.9	52.1	51.7	29.6	29.5
CFD5	0.00	0.00	1.00	98.9	98.9	97.5	97.5	56.2	56.3	37.0	37.0
CFD6	0.33	0.33	0.33	99.5	99.5	98.0	98.1	50.7	51.7	31.6	31.9
CFD7	0.17	0.67	0.17	99.7	99.7	98.3	98.3	52.5	52.1	34.4	34.3

The regression models of the four responses were established by linear regression fitting (Equations (3)–(6)), as follows:

$$Y_1 \text{ (Turbidity)} = 99.5038X_1 + 99.6038X_2 + 98.9038X_3 + 0.391X_1X_2 - 0.209X_1X_3 + 1.591X_2X_3; R^2 = 99.5\%; R^2 \text{ adjusted} = 97.3\%. \quad (3)$$

$$Y_2 \text{ (TSS)} = 97.9083X_1 + 98.3083X_2 + 97.5083X_3 + 0.10X_1X_2 + 0.10X_1X_3 + 1.30X_2X_3; R^2 = 97.9\%; R^2 \text{ adjusted} = 87.7\%. \quad (4)$$

$$Y_3 \text{ (COD)} = 48.61X_1 + 54.41X_2 + 56.31X_3 + 19.8X_1X_2 + 3.6X_1X_3 - 36.0X_2X_3; R^2 = 95.5\%; R^2 \text{ adjusted} = 73.1\%. \quad (5)$$

$$Y_4 \text{ (TOC)} = 31.635X_1 + 28.435X_2 + 37.035X_3 + 57.44X_1X_2 - 51.76X_1X_3 - 9.76X_2X_3; R^2 = 99.7\%; R^2 \text{ adjusted} = 98.1\%. \quad (6)$$

Validation of the statistical design model is a very important parameter, in order to assess the relevance of the obtained results. Univariate analysis of variance (ANOVA) provides an extremely powerful and useful tool for the statistical tests of different factors and their interactions in experiments [58]. The regression-adjusted average squares and linear regression-adjusted average squares, allowed the calculation of the Fisher ratios (F-value), which allowed the determination of the statistical significance (*p*-value). Table S1 (see Supplementary Materials) shows that the P-value for regression, linear regression and quadratic regression of turbidity, TSS, COD, and TOC, is non-significant for a $p < 0.05$ [59].

To establish the reliability of the results that were obtained by the SLD statistic design, it was necessary to evaluate other sets of parameters. By the performance of linear fit, the regression equations were obtained. These equations established a relation between the observed results and the predicted results, which were evaluated by the calculation of R^2 and R^2 adjusted. By observation of the R^2 values, turbidity, TSS, COD, and TOC had values of 99.5, 97.9, 95.5, and 99.7%, respectively, which were greater than 80.0%, ensuring a very good model fit [60,61]. The R^2 adjusted that was obtained from the turbidity, TSS, COD, and TOC regression equations (97.3, 87.7, 73.1, and 98.1%, respectively), was also high, indicating the strong significance of the model [61,62].

The adequacy of the model was also evaluated by use of diagnostic plots, such as a normal probability plot of the standardized residuals, and the plot between individual residual values and the fitted values (Figure 3). The normal probability plot shows the distribution of the residual value, which is defined as the difference between the predicted (model) and observed (experimental) values. From the normal probability plot, the population is claimed not to be normally distributed if, and only if, the n points do not fall close to a straight line [63].
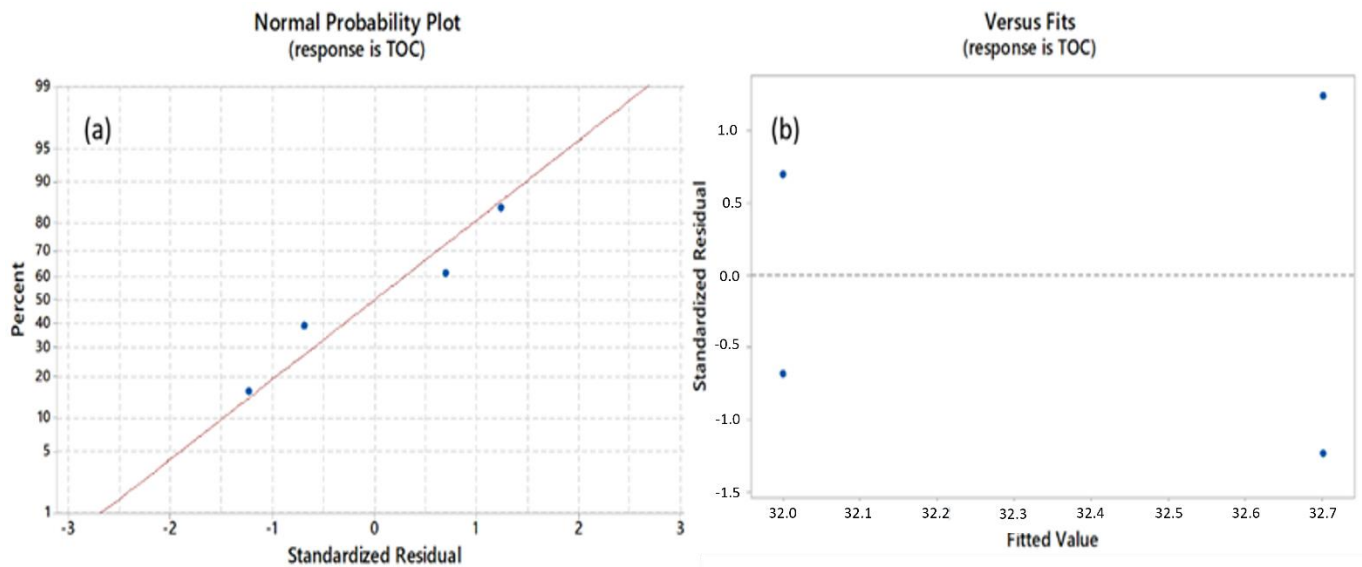
Int. J. Environ. Res. Public Health **2021**, 18, 8882

9 of 26

Figure 3. (**a**) Normal probability plot, (**b**) residual versus the fitted value of the data after CFD process, with TOC as response.

In Figure 3, the formation of a straight line was observed and the residual values were normally distributed on both sides of the line, which indicated that the experimental points of turbidity, TSS, COD, and TOC were reasonably aligned with the predicted values.

After analyzing the plots between individual residual values and the fitted values, it was observed that the turbidity, TSS, COD, and TOC residual values were scattered randomly around zero, which was similar to Harbi et al. [64], who observed a uniform scattering of the residual values after the performance of an SLD statistic design on a PCR detection method for nitrite reductase genes.

3.1.2. Simplex Lattice Design—Model Optimization

To improve the CFD optimization, an SLD statistic design was performed, in which three different coagulants, potassium caseinate (X_1), activated sodium bentonite (X_2), and PVPP (X_3), were tested under seven different combinations, with the evaluation of turbidity, TSS, COD, and TOC (Table 5), under the following operational conditions: pH 4.0, rapid mixing 150 rpm/3 min, slow mixing 20 rpm/20 min, temperature 298 K, and sedimentation period 12 h. The maximum dosage (1.0 g/L) and pH 4.0 were selected, based on the works of Cosme et al. [65,66], who performed coagulation with these coagulants on the natural pH (3.3–3.6) of wine. Additionally, potassium caseinate has an isoelectric point of 4.6 [67] and, at a pH higher than 4.6, potassium caseinate is dissolved. The activated sodium bentonite that was used in this work presents a pH of 7.4, which corresponds to its isoelectric point (pH = 7); however, bentonite becomes electropositive at pH 3.6–4.0 [68] and, therefore, after bentonite addition to the wastewater, its pH was corrected to 4.0. The variable charge of clays is affected by the pH, due to the ionization of its external hydroxyl groups. Therefore, the external sites may acquire positive (OH_2^+) or negative charge ($\_O^-$), whether the pH is lower or higher than its isoelectric point (pH at the point of zero charge) [69,70]. In the work of Guimarães et al. [69], when the clay was mixed with WW at pH 4.0, a mechanism of adsorption occurred, in which a high concentration of amphoteric flavylium species were adsorbed by the clay. Therefore, pH 4.0 is the best pH for the performance of the CFD process, with activated sodium bentonite. The PVPP was tested in this work, based on the research of Labord et al. [71], in which it was reported that PVPP had a high affinity for polyphenols, according to tests conducted in wine treatment. PVPP is a high-molecular-weight polymer, which is insoluble in water [38]. It interacts with polyphenols via H bonds between their CO-N linkages and phenol groups [72].

Figure 4 shows the interactions of activated sodium bentonite, potassium caseinate, and PVPP, with the colloids present in the wastewater. When bentonite was added, a

mechanism of adsorption and charge neutralization occurred, attracting the colloids present in the WW to the interlayer region of the clay [73]. A similar mechanism was observed with the employment of potassium caseinate, which due to the different charges, attracted the negatively chargeed particles to the positively charged proteins, producing heavy aggregated particles, which precipitate by gravity [74]. PVPP acted by a mechanism of adsorption and interparticle bridging. The polymer chains of PVPP adsorbed the colloids from the WW, as a result of (1) coulombic (charge–charge) interactions, (2) dipole interaction, (3) hydrogen bonding, and (4) van der Waals forces of attraction [75]. In addition, PVPP creates a tridimensional net that adsorbs on the available surface sites of other particles (such as bentonite and potassium caseinate), thus creating a "bridge" between the particles surfaces, resulting in larger particles that settle more efficiently by gravity.
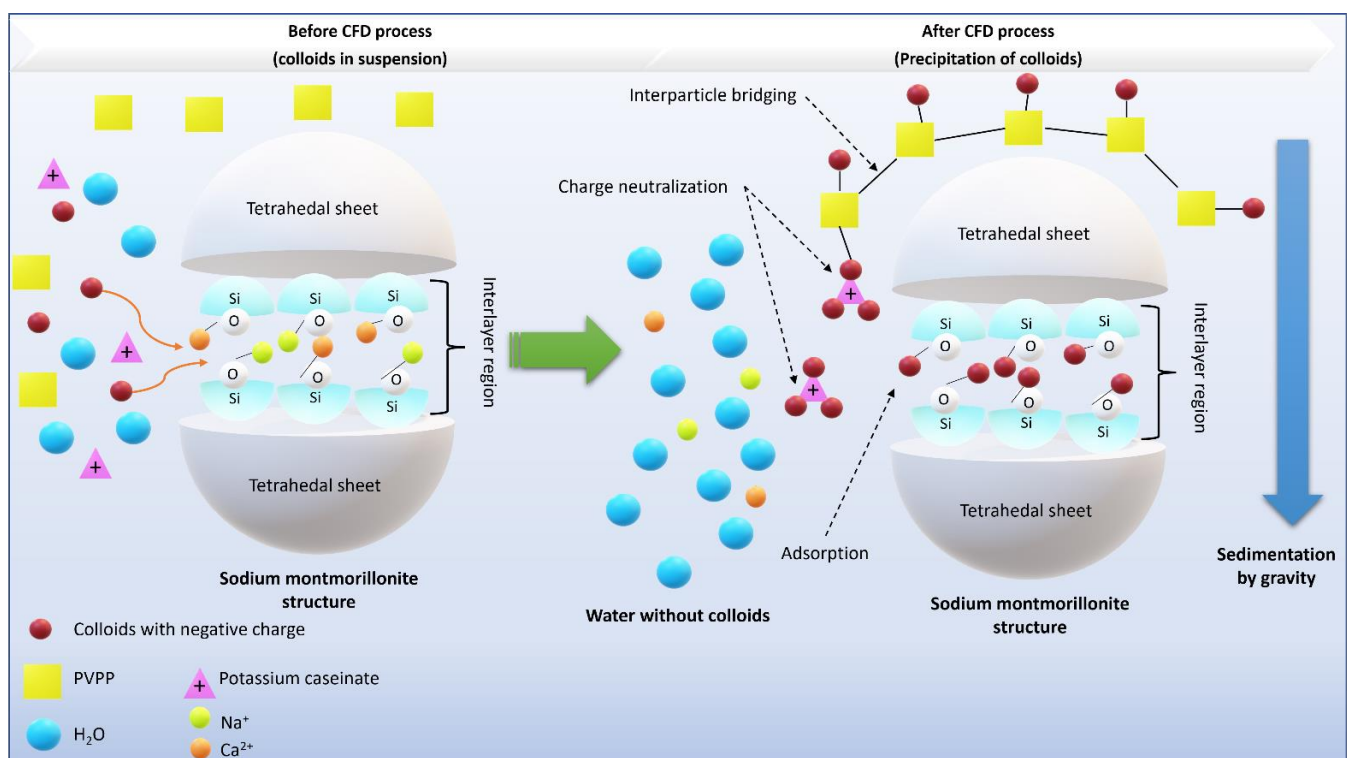

Figure 4. Mechanism of colloid removal by activated sodium bentonite, potassium caseinate and PVPP.

The statistical analysis that was obtained from the SLD design was converted into an optimization chart, which related the best results that were obtained from the CFD process. In accordance with the optimization chart (Figure S1), the mixture of 0.48 g/L potassium caseinate (X_1) and 0.52 g/L bentonite (X_2) could reach a maximum removal of COD, TOC, turbidity, and TSS of 56.5, 44.3, 99.6, and 98.1%, respectively. Therefore, the optimal conditions that were selected for the CFD process were as follows: 0.48 g/L potassium caseinate, 0.52 g/L bentonite, pH 4.0, temperature 298 K, rapid mix 150 rpm/3 min, slow mix 20 rpm/20 min, and sedimentation time 12 h. After 12 h of sedimentation (Table S2, Figure 5), a 98.3, 97.6, 48.0, and 44.6% removals of turbidity, TSS, COD, and TOC were observed, which are similar to the values predicted by the optimization chart in Figure S1. Considering the Portuguese Decree Law n° 236/98 for residual water discharge, it was observed that TSS achieved the legal value (60 mg/L).
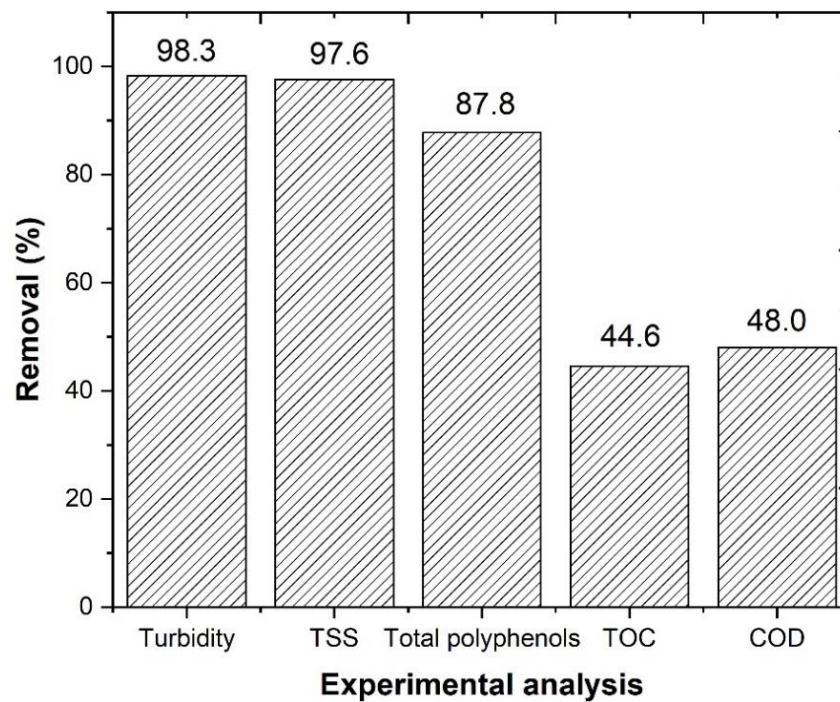
Figure 5. Overall results after coagulation–flocculation–decantation process (CFD). Operational conditions: 0.48 g/L potassium caseinate, 0.52 g/L bentonite, pH 4.0, temperature 298 K, rapid mix 150 rpm/3 min, slow mix 20 rpm/20 min an 12 h of sedimentation time.

3.2. Ozonation Experiments

3.2.1. Effect of pH

In Section 3.1, the CFD process was optimized by employing an SLD statistical design. However, the CFD process was insufficient to substantially decrease the high organic carbon content that was present in the WW, thus, the application of a further chemical oxidation process, based on the reaction between ozone and a catalyst (Fe^{2+}), under UV-C radiation, was necessary. In the work of Huang et al. [76], it was observed that a combination of iron with O_3 reached higher dissolved organic carbon (DOC) removal (53%), regarding O_3 alone (32%), in the treatment of pharmaceutical wastewater. However, to our knowledge, the $O_3/Fe^{2+}/UV-C$ process was never applied to the treatment of WW. Therefore, the $O_3/Fe^{2+}/UV-C$ process was optimized, to act as a CFD complementary process. In order to maximize TOC removal, different pH's (4.0, 7.0, 9.0, and 11.0) were tested, under the following operational conditions: $[Fe^{2+}]$ = 1.0 mM, ozone flow rate 5 mg/min, air flow 1.0 L/min, agitation 350 rpm, time 600 min, and a UV-C mercury lamp (254 nm). In Figure 6, the $O_3/Fe^{2+}/UV-C$ system is represented in closed symbols, while the blank experiments, at pH 4.0 (O_3, UV-C, and $O_3/UV-C$), are represented in open symbols. The effect of the pH in the blank experiments is shown in Table S3. It was observed that with different initial pH (4.0, 7.0, 9.0, and 11.0), there was a TOC removal of 31.9, 28.6, 11.2, and 35.8%, respectively, for O_3; 33.1, 0.9, 0.0, and 4.1%, respectively, for UV-C; and 57.5, 37.6, 36.5, and 38.0%, respectively, for $O_3/UV-C$. These results were in agreement with the work of Hassanshahi and Karimi-Jashni [77], which observed that the pH had little effect in the COD removal of gray water, by the ozonation process.
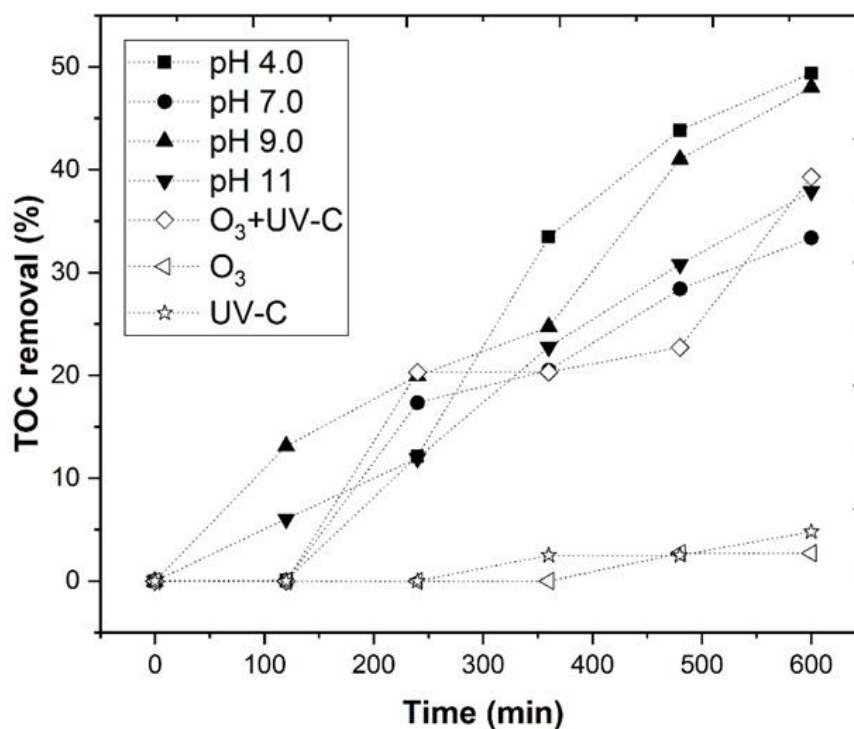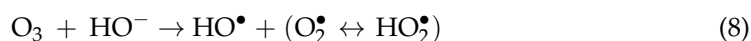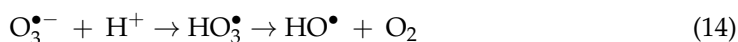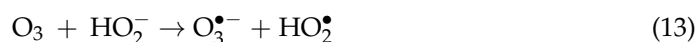
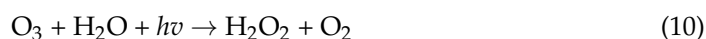*Int. J. Environ. Res. Public Health* **2021**, *18*, 8882

12 of 26

Figure 6. Evaluation of TOC removal through the $O_3/Fe^{2+}/UV$-C process at different pH values (4.0–11.0). The following ozonation experimental conditions: $[Fe^{2+}]$ = 1.0 mM, ozone flow rate 5 mg/min, air flow 1.0 L/min, agitation 350 rpm, time 600 min, radiation UV-C mercury lamp (254 nm). Blank experiments (O_3/UV-C, O_3 and UV-C—pH 4.0) are also shown as a reference.

The results in Figure 6 showed a lower TOC removal efficiency for a single O_3 application, regarding O_3/UV-C. These results can be explained by two mechanisms through which ozone can degrade organic pollutants, such as direct electrophilic attack (Equation (7)) and indirect attack, through the formation of hydroxyl radicals (Equations (8) and (9)) [78,79], which are shown as follows:

$$O_3 + R \rightarrow R_{OX} \tag{7}$$

$$O_3 + HO^- \rightarrow HO^\bullet + (O_2^\bullet \leftrightarrow HO_2^\bullet) \tag{8}$$

$$HO^\bullet + R^\bullet \rightarrow R'_{OX} \tag{9}$$

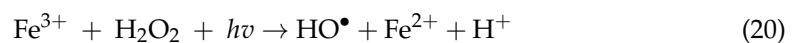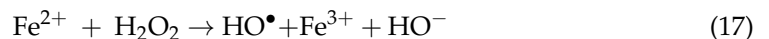where R is the organic solutes and Rox is the oxidized organic products.

With the application of UV-C radiation at 254 nm, in combination with O_3, the TOC removal increased, because ozone absorbs UV-C light [80,81] and the formation of H_2O_2, by ozone photolysis occurs, which, in turn, produced hydroxyl radicals ($HO^\bullet$), as observed in Equations (10)–(14) [82] as follows:

$$O_3 + H_2O + h\nu \rightarrow H_2O_2 + O_2 \tag{10}$$

$$H_2O_2 + h\nu \rightarrow 2HO^\bullet \tag{11}$$

$$H_2O_2 \leftrightarrow HO_2^- + H^+ \tag{12}$$

$$O_3 + HO_2^- \rightarrow O_3^{\bullet-} + HO_2^\bullet \tag{13}$$

$$O_3^{\bullet-} + H^+ \rightarrow HO_3^\bullet \rightarrow HO^\bullet + O_2 \tag{14}$$

Agustina et al. [79] also observed two more reactions that occurred under O_3/UV-C, as described in Equations (15) and (16) as follows:

$$HO_2^{\bullet} \rightarrow O_2^{\bullet -} + H^+ \tag{15}$$

$$O_3 + O_2^{\bullet -} \rightarrow O_3^{\bullet -} + O_2 \tag{16}$$

With the application of the O_3/Fe^{2+}/UV-C system, a TOC removal of 63.2%, 42.4%, 52.7%, and 49.6%, respectively, was observed, for pH 4.0, 7.0, 9.0, and 11.0. In Equation (10), it was observed that the photolysis of O_3 could produce H_2O_2. When Fe^{2+} was added, the catalyst decomposed the H_2O_2, producing $HO^{\bullet}$ radicals (Equations (17)–(19)) [83,84], thus increasing the rate of TOC removal. With the application of UV-C radiation, the regeneration of Fe^{3+} to Fe^{2+} (Equation (20)) took place [85,86], explaing the high efficiency of the system.

$$Fe^{2+} + H_2O_2 \rightarrow HO^{\bullet} + Fe^{3+} + HO^- \tag{17}$$

$$Fe^{3+} + H_2O_2 \rightarrow FeHO_2^{2+} \tag{18}$$

$$FeHO_2^{2+} \rightarrow HO_2^{\bullet} + Fe^{2+} \tag{19}$$

$$Fe^{3+} + H_2O_2 + hv \rightarrow HO^{\bullet} + Fe^{2+} + H^+ \tag{20}$$

The TOC removal results fitted a pseudo-first-order kinetic rate (Equation (21)) [87].

$$\ln \frac{[TOC]_t}{[TOC]_0} = -kt \tag{21}$$

where $[TOC]_0$ and $[TOC]_t$ are the TOC concentrations at time 0 and t in mg C/L.

As the O_3/Fe^{2+}/UV-C reaction proceeds, the concentration of TOC decreases. Another measure of the rate of a reaction, relating concentration to time, is the half-life, $t_{1/2}$, which is the time required for the concentration of TOC to decrease to half of its initial concentration. We can obtain an expression for $t_{1/2}$, for a first-order reaction, as described by Equation (22) [87], as follows:

$$t_{1/2} = \frac{0.693}{k} \tag{22}$$

It was observed that $k_{pH\ 4.0} = 1.67 \times 10^{-3}$ min^{-1} > $k_{pH\ 9.0} = 1.18 \times 10^{-3}$ min^{-1} > $k_{pH\ 11} = 1.07 \times 10^{-3}$ min^{-1} > $k_{pH\ 7.0} = 9.41 \times 10^{-4}$ min^{-1}. The decrease in the kinetic rate, with the increase in pH > 4.0, could be explained by the precipitation of iron at alkaline pH, in the form of iron hydroxide ($[Fe^{2+}]$ leached = 12.6, 35.4, 42.6, and 188.8 mg Fe/L, respectively, for pH 4.0, 7.0, 9.0, and 11), which decreases the conversion of H_2O_2 to $HO^{\bullet}$ and reduces the transmission of the radiation [88]. Therefore, based in these results, pH 4.0 was selected as the best pH for the O_3/Fe^{2+}/UV-C process studied.

3.2.2. Effect of Fe^{2+} Concentration

In the previous section, as the pH had a great influence on the removal of TOC from the WW, by the ozonation process, was described. It was also observed that the treatment using the combination of O_3/UV-C generated H_2O_2, which interacted with Fe^{2+} to produce $HO^{\bullet}$ radicals. Therefore, in this section, the Fe^{2+} concentration was varied (0.5–2.0 mM) under the following operational conditions: pH 4.0, ozone flow rate 5 mg/min, air flow 1.0 L/min, agitation 350 rpm, and radiation UV-C mercury lamp (254 nm).

In Figure 7, a TOC removal of 59.0, 63.2, and 66.7% (Table S4), was observed, for 0.5, 1.0, and 2.0 mM Fe^{2+}, respectively. These results agreed with Quiroz et al., [89], who stated that the application of iron with ozone improved the COD removal of industrial wastewater. In addition, in the work of Piera et al. [82], it was reported that Fe^{2+} can interact with O_3 and produce $HO^{\bullet}$ radicals (Equations (23) and (24)), as follows:

$$Fe^{2+} + O_3 \rightarrow FeO^{2+} + O_2 \tag{23}$$

$$FeO^{2+} + H_2O \rightarrow Fe^{3+} + HO^{\bullet} + HO^{-} \tag{24}$$
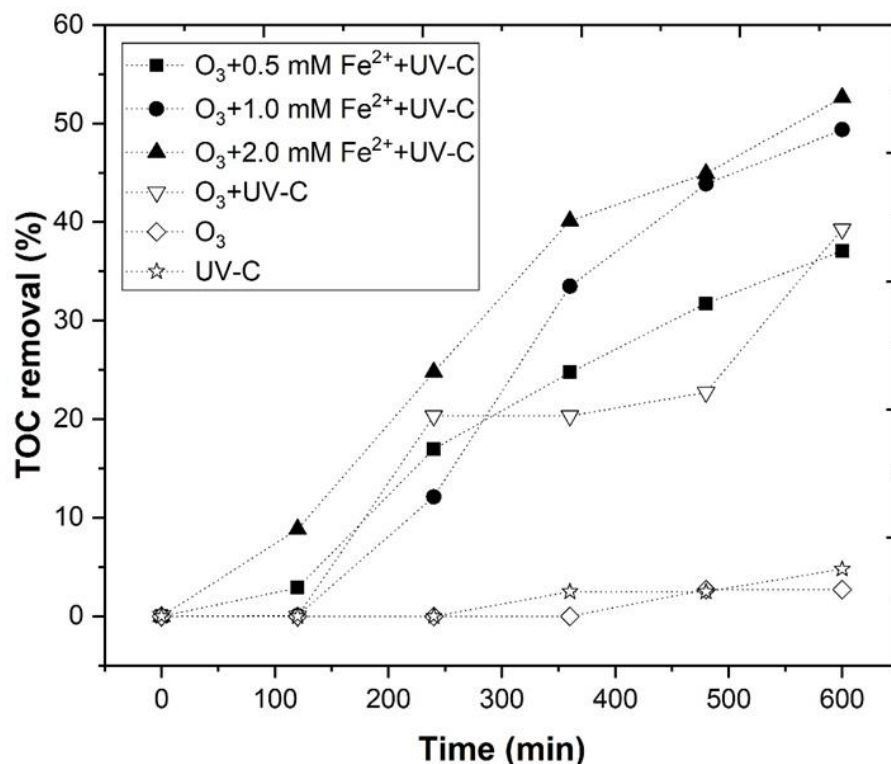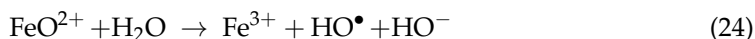
Figure 7. Evaluation of TOC removal through the $O_3/Fe^{2+}/UV\text{-}C$ process at different Fe^{2+} concentrations (0.5–2.0 mM). Ozonation experimental conditions were as follows: pH = 4.0, ozone flow rate 5 mg/min, air flow 1.0 L/min, agitation 350 rpm, time 600 min, radiation UV-C mercury lamp (254 nm). Blank experiments ($O_3/UV\text{-}C$, O_3, and UV-C—pH 4.0) are also shown as a reference.

After 600 min of reaction, an Fe^{2+} concentration of 1.84, 12.60, and 41.92 mg Fe/L, respectively, was observed, for 0.5, 1.0, and 2.0 mM. With the application of 0.5 mM Fe^{2+}, there was a low concentration of Fe^{2+} present in the solution, to react with H_2O_2. The use of higher concentrations of ferrous iron resulted in a higher TOC removal, although the increase from 1.0 to 2.0 mM Fe^{2+} was very mild, possibly because scavenging reactions, between Fe^{2+} and $HO^{\bullet}$ radicals, may have occurred, as observed in Equations (25)–(26) [19], as follows:

$$Fe^{2+} + HO^{\bullet} \rightarrow Fe^{3+} + HO^{-} \tag{25}$$

$$Fe^{2+} + HO_2^{\bullet} \rightarrow Fe^{3+} + HO_2^{-} \tag{26}$$
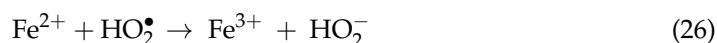
The results were fitted into a pseudo-first-order kinetic rate, and the following order was observed: $k_{2.0\text{ mM}} = 1.72 \times 10^{-3}$ min^{-1} > $k_{1.0\text{ mM}} = 1.67 \times 10^{-3}$ min^{-1} > $k_{0.5\text{ mM}} = 1.34 \times 10^{-3}$ min^{-1}. Due to the low differences in the kinetic rate that was observed between 1.0 and 2.0 mM Fe^{2+}, and due to the high costs that are associated with the application of 2.0 mM Fe^{2+}, a ferrous iron concentration of 1.0 mM was selected as the best concentration for the $O_3/Fe^{2+}/UV\text{-}C$ process.

Bolton et al. [90] proposed figures of merit for electric-driven photocatalysis. For first-order kinetics, they proposed the electric energy per order (E_{EO}) as the electric energy, in kWh that are required to reduce the concentration of a pollutant concentration C by one order of magnitude, according to Equation (27), where P is the rated power [kW] of the

AOP system, V is the volume [L] of water or air treated in the time t [h], and TOC_i and TOC_f are the concentrations of total organic carbon at initial and t times.

$$E_{EO} = \frac{P * t * 1000}{V * \log\left(\frac{TOC_i}{TOC_f}\right)} \text{ Batch operation} \qquad (27)$$

The results are presented in Table 6 and, as expected by increasing the Fe^{2+} concentration, the E_{EO} values decreased. Lower E_{EO} values (in $kWh \cdot m^{-3} \cdot order^{-1}$) correspond to higher removal efficiencies, in terms of electrical power consumption [90]. The application of UV-C radiation alone achieved the lowest E_{EO} value (1720 $kWh \cdot m^{-3} \cdot order^{-1}$) in comparison to the O_3/UV-C and O_3 alone (2153 and 2996 kWh $m^{-3} \cdot order^{-1}$, respectively), due to the low power of the UV mercury lamp. However, the reaction kinetics of the UV-C alone, were much lower ($k_{UV-C} = 7.17 \times 10^{-4}$ min^{-1}) in comparison to the other treatments, thus more energy will be required to achieve similar TOC degradation. With the application of the O_3/Fe^{2+}/UV-C system, the results in Table 6 clearly indicated that with 0.5 mM Fe^{2+}, the reaction took too much time, increasing the electric power consumption. However, little differences in the E_{EO} values were observed when 1.0 and 2.0 mM Fe^{2+} were applied, and, considering the high iron leaching that was observed with 2.0 mM Fe^{2+}, the application of 1.0 mM Fe^{2+} becomes the best choice.

Table 6. Evaluation of first-order kinetic rate (k), half-life ($t_{1/2}$) and electric energy per order (E_{EO}) through the O_3/Fe^{2+}/UV-C process at different Fe^{2+} concentrations (0.5–2.0 mM). $P_{Ozonator} = 0.025$ kW, $P_{UV-C} = 0.015$ kW, $t = 10$ h, V = 0.5 L.

[Fe^{2+}]	k	$t_{1/2}$	E_{EO}
mM	(min^{-1})	(min)	($kWh \cdot m^{-3} \cdot order^{-1}$)
UV-C	7.17×10^{-4}	966.5	1720
O_3/UV-C	1.31×10^{-3}	529.0	2153
O_3	6.86×10^{-4}	1009.9	2996
O_3/0.5 mM Fe^{2+}/UV-C	1.34×10^{-3}	517.2	2065
O_3/1.0 mM Fe^{2+}/UV-C	1.67×10^{-3}	414.9	1843
O_3/2.0 mM Fe^{2+}/UV-C	1.72×10^{-3}	402.9	1677

The comparative values of E_{EO}, for the degradation of active pharmaceutical ingredients, real textile wastewater, and organic pollutants, by the ozonation process, are displayed in Table 7. In addition, a comparative study is also shown, in which the winery wastewater was treated by a UV-C/PMS/Co(II) system. The results showed that the winery wastewater is very difficult to treat (1843 kWh $m^{-3} \cdot order^{-1}$), with higher energy requirements, regarding the treatment of active pharmaceutical ingredients, real textile wastewater, and organic pollutants. These results were in agreement with Rodriguez-Chueca et al. [19], who observed a high E_{EO} for the treatment of WW (173 $kWh \cdot m^{-3} \cdot order^{-1}$). The application of ozonation processes in the treatment of WW is insufficient, with scarce examples of organic matter removal and energy consumption. Most of the authors studied the degradation of emerging contaminants and textile dye removal [91–93]; however, the degradation of the organic matter load of winery wastewater requires more demanding treatments, with higher energy consumption [20].

3.2.3. Evaluation of Ozone Consumption

In the previous sections, we described how to optimize the ozonation process, and it was observed that under the best operational conditions, pH 4.0, [Fe^{2+}] = 1.0 mM, ozone flow rate 5 mg/min, air flow 1.0 L/min, agitation 350 rpm and UV-C radiation (254 nm), a TOC removal of 63.2% was achieved. However, to understand the efficiency of the O_3/Fe^{2+}/UV-C process, the concentration of ozone dissolved in the wastewater was assessed (Table S5). The rate of ozone consumption was monitored by AccuVac Ampul procedure, and the ozone that was lost in the process was measured by the difference

between the ozone mass flow rate at the inlet of the reactor and the ozone dissolved in the WW.

Table 7. Reported values of electric energy per order (E_{EO}) in ozonation processes.

Wastewater Type	AOP Process	Observations	E_{EO} (kWh·m^{-3}·order^{-1})	References
Winery wastewater	UV-C (254 nm)/PMS/Co(II)	[PMS] = 2.5 mM [Co(II)] = 1.0 mM t = 90 min TOC$_i$ = 143 mg C/L	173	[19]
Active pharmaceutical ingredients (APIs)	UV-C/O_3	Gas flow = 3.2 L/min t = 30 min TOC$_i$ = 21.5 mg C/L	1.50	[91]
Real textile wastewater	Direct ozonation	Gas flow = 1.4 L/min t = 9 min TOC$_i$ = 169 mg C/L	2.43	[92]
Organic pollutants	UV-C (254 nm)/O_3	Gas flow = 0.4 L/min t = 15 min TOC$_i$ = 79 mg C/L	29.10	[93]
	UV-C (254 nm)/TiO_2/O_3	Gas flow = 0.4 L/min t = 20 h TOC$_i$ = 79 mg C/L	10.23	
Winery wastewater	Fe^{2+}/O_3/Fe^{2+}/UV-C (254 nm)	Gas flow = 1.0 L/min [Fe^{2+}] = 1.0 mM t = 10 h TOC$_i$ = 1962 mg C/L	1843	Present results

In Figure 8, it was observed that under a constant injection of 5 mg O_3/L, only 0.165, 0.330, 0.190, 0.270, and 0.360 mg O_3/min reacted with the Fe^{2+}, to produce hydroxyl radicals (HO$^\bullet$), respectively, at time of 120, 240, 360, 480, and 600 min^{-1}. This concentration of dissolved O_3 was observed to be much lower than the concentration that was observed in the work of Lucas et al. [23], considering that the air was supplied by a small air pump, but a high TOC removal kinetic rate was observed with this process.

3.3. Combination of Coagulation–Flocculation–Decantation with Ozonation Processes

The WW is very toxic when discharged into the environment without proper treatment, due to the high levels of organic carbon that are present in its composition (Table 1). Previous treatments, with CFD and O_3/Fe^{2+}/UV-C, achieved a high TOC removal; however, both treatments showed limitations and, therefore, in this section, the processes of CFD and O_3 were combined CFD/O_3 and O_3/CFD processes, with the application of the CFD process' best operational conditions—0.48 g/L potassium caseinate, 0.52 g/L bentonite, pH 4.0, temperature 298 K, rapid mix 150 rpm/3 min, slow mix 20 rpm/20 min, and sedimentation time 12 h—and the ozonation process' best operational conditions—pH 4.0, [Fe^{2+}] = 1.0 mM, ozone flow rate 5 mg/min, air flow 1.0 L/min, agitation 350 rpm, and UV-C radiation (254 nm).

Figure 9 shows a TOC removal of 63.2 and 66.1%, respectively, after the performance of O_3 and the combined O_3/CFD processes (Table S6). A TOC removal of 44.6 and 65.5%, respectively, was also observed, after the performance of CFD and the CFD/O_3 processes. Clearly, there were not significant differences between both the combined treatments; however, after the analysis of the biodegradability, an increase, from 0.28 (raw WW) to 0.29 for O_3/CFD and 0.40 for CFD/O_3, was observed. Therefore, the application of CFD before the O_3 process can be more advantageous for the WW treatment. These results were in agreement with Liu et al. [94], who observed that the performance of the CFD process, as a pre-treatment, enhanced the ozonation process in the treatment of a landfill leachate. The results were also in agreement with Bu et al. [95], who observed that the performance of the CFD process, as a pre-treatment, followed by ozonation, enhanced the UV$_{254}$ removal efficiency and decreased the accumulation of organic matter in the

treatment of wastewater. Considering the Portuguese Decree Law nº 236/98 for residual water discharge, only TSS achieved the legal value (60 mg/L), while COD (150 mg O_2/L), BOD_5 (40 mg O_2/L), and total polyphenols (0.5 mg gallic acid/L), failed to reach the legal thresholds. Nonetheless, the observed improvement in biodegradability showed that the WW can be sent to a biological reactor for further degradation of organic matter.
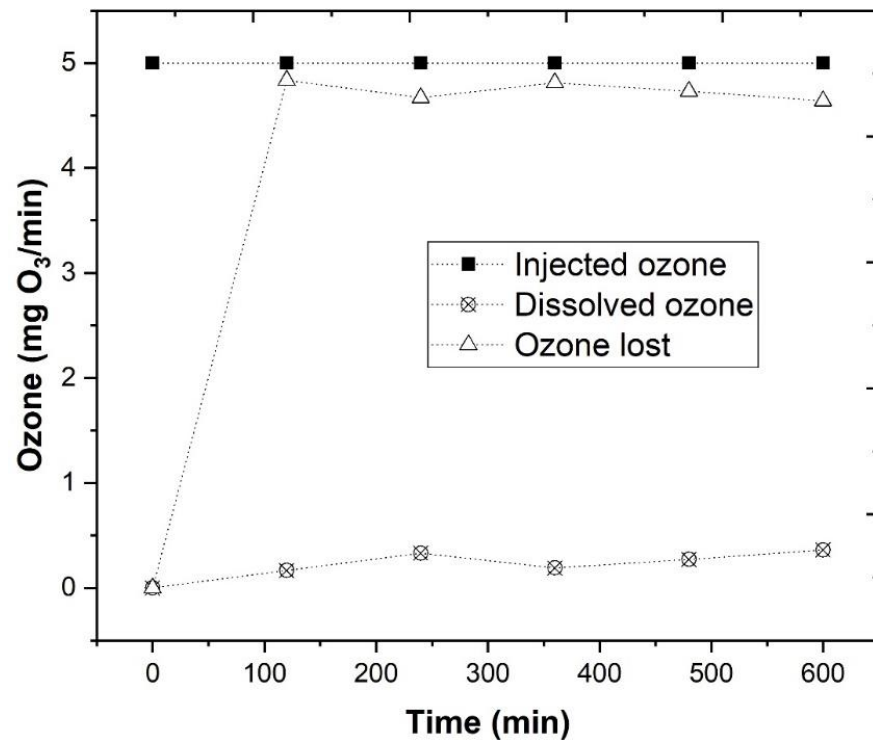

Figure 8. Evaluation of the O_3 concentration dissolved within the WW, by application of the indigo ozone reagent. O_3/Fe^{2+}/UV-C experimental conditions were as follows: pH = 4.0, [Fe^{2+}] = 1.0 mM, ozone flow rate 5 mg/min, air flow 1.0 L/min, agitation 350 rpm, time 600 min, radiation UV-C mercury lamp (254 nm).

A factor that possibly explains the high organic carbon removal that was observed after the combined O_3/CFD and CFD/O_3 processes, is the reduction in turbidity, TSS, and total polyphenols, which would otherwise prevent light from penetrating into the water and triggering the photo-Fenton reaction [11]. In Figure 10, the application of O_3, O_3/CFD, CFD, and CFD/O_3, achieved a turbidity removal of 65.5, 99.9, 98.3, and 99.3%, respectively, and a TSS removal of 66.8, 98.3, 97.6, and 98.3%, respectively. In addition to turbidity and TSS, a total polyphenol removal of 95.1, 95.9, 81.2, and 99.3%, respectively, was also observed. These results were in agreement with Lucas et al. [23], who observed that the ozonation process could be beneficial for the removal of polyphenols (toxicity) from the winery wastewater, thus contributing to the safety of public and environmental health.

3.4. Effect of the Treatments in Phytotoxicity of Different Plants

In previous sections, was described how the combination of the CFD and ozonation processes were beneficial for the reduction in the organic carbon present in the WW. However, considering that the application of oenological coagulants in combination with the ozonation process, has never been implemented in wastewater treatment, its effects in vegetables are still unknown. Therefore, in this section, we evaluated the effects of the different treatments in the phytotoxicity of different species of vegetables. A series of tests were performed on the germination of seeds, in order to evaluate the phytotoxicity of the treatments, similarly to several authors [96–99], in two Dicotyledonae species (lettuce and cucumber) and in two Monocotyledonae species (corn and onion). In Figure 11, it was

observed that WW had a phytotoxic effect on cucumber and lettuce seeds (GI = 51 and 0%, respectively). The performance of the treatments O_3, O_3/CFD, CFD, and CFD/O_3 increased the germination index (GI) of the cucumber seeds, to 113, 109, 71, and 117% (Table S7), respectively. The germination index of the lettuce seeds increased to 298, 88, and 249%, respectively, for O_3, O_3/CFD, and CFD/O_3. These are excellent values that reveal the goodness of the studied treatments and the reduction in phytotoxicity.
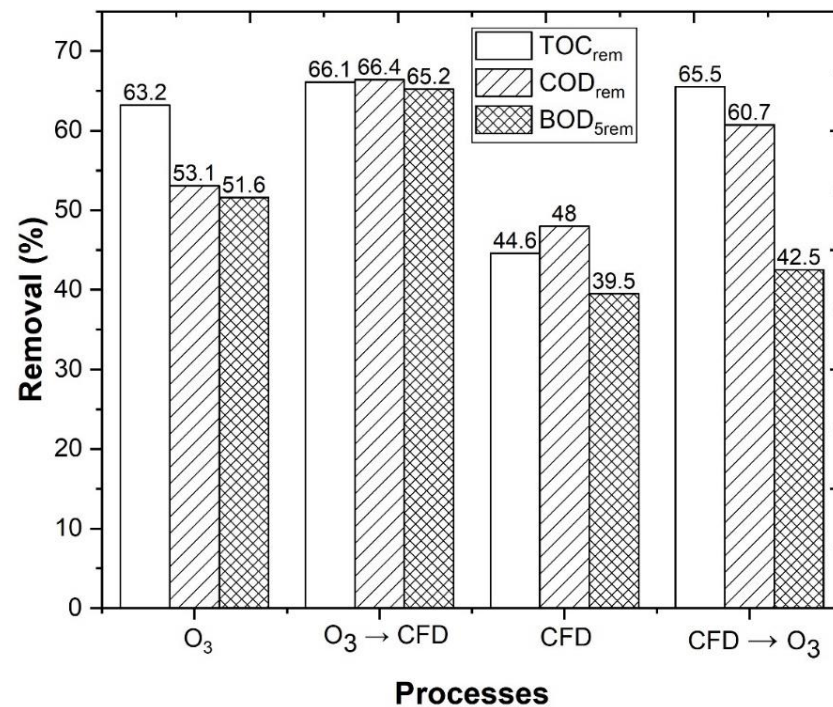
Figure 9. TOC, COD and BOD_5 removal. CFD operational conditions, as follows: 0.48 g/L potassium caseinate, 0.52 g/L bentonite, pH 4.0, temperature 298 K, rapid mix 150 rpm/3 min, slow mix 20 rpm/20 min, sedimentation time 12 h. O_3/Fe^{2+}/UV-C experimental conditions, as follows: pH = 4.0, [Fe^{2+}] = 1.0 mM, ozone flow rate 5 mg/min, air flow 1.0 L/min, agitation 350 rpm, time 600 min, radiation UV-C mercury lamp (254 nm).

As previously observed, some of the problems that are generated by this type of wastewater are the intense color and high turbidity, which absorbs the radiation and decreases the treatment efficiency. The intense color that is present in winery wastewaters appears mainly due to the presence of total phenols, non-flavonoids, flavonoids, total anthocyanins, colored anthocyanins, total pigments, and total tannins, present in the wines [100]. Considering that there is insufficient information regarding the impact of the CFD and ozonation processes in the phenolic composition of the WW, in this section, the efficiency of these treatments in the removal of total phenols, non-flavonoids, flavonoids, total anthocyanins, colored anthocyanins, total pigments, and total tannins, was evaluated (Figure 12). The performance of the treatments O_3, O_3/CFD, CFD, and CFD/O_3 achieved a total phenol removal of 0.0, 5.1, 1.9, and 3.2%, respectively, a non-flavonoid removal of 0.0, 0.0, 2.6, and 2.6%, respectively, and a flavonoid removal of 0.0, 14.6, 0.0, and 7.3% (Table S8), respectively, which are responsible for the yellow color in wines [38]. In Figure 12, a high decrease in the total anthocyanins (50.0, 50.0, 25.0, and 100%, respectively) and colored anthocyanins (28.6, 10.0, 42.9, and 100%, respectively) was observed, which are linked to the red color of wines [101]. The reduction in these phenolic compounds had an effect in the removal of color from the wastewater, which was evaluated by a CIELab analysis (Table S9). The combined treatments O_3/CFD and CFD/O_3 had negative values for Δa^* and Δb^* (−1.90 and −3.29), which indicated a reduction in the red and yellow color. The luminosity (L^*) increased from 0.0% (raw WW) to 99.7 and 100%, respectively, which

Int. J. Environ. Res. Public Health **2021**, *18*, 8882

19 of 26

meant that the phenolic compounds were directly linked to the dark-yellow color of the wastewater. The color removal, given by the Euclidean distance, was 99.74 and 100, after the combined treatments of O_3/CFD and CFD/O_3, which meant that color removal was perceptible by the human eye, which is in accordance with Spagna et al. [41].
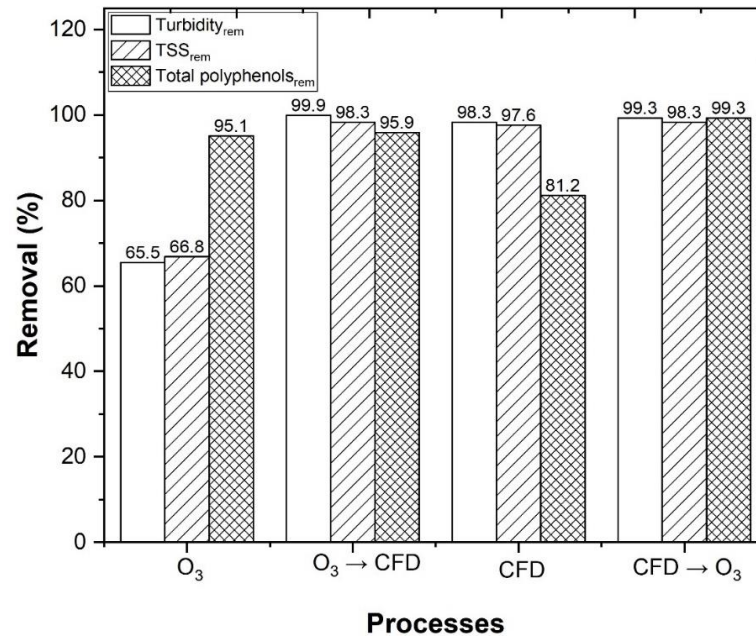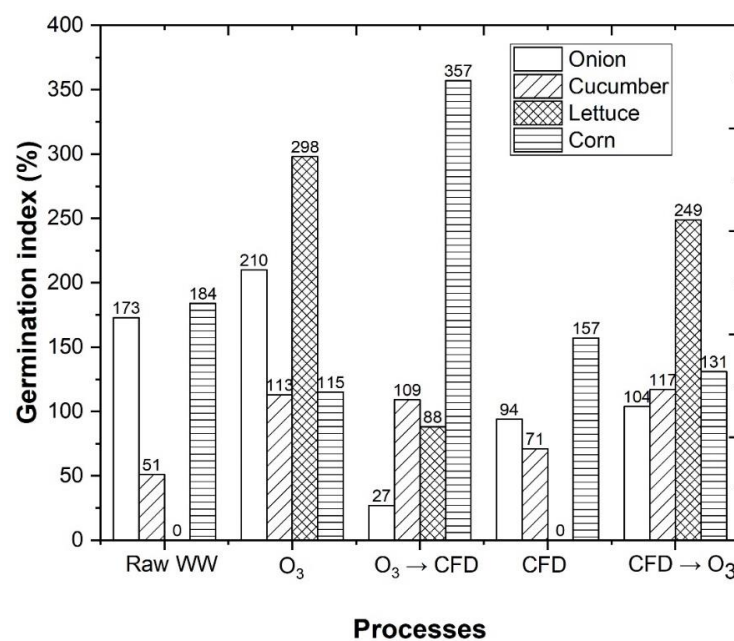

Figure 10. Turbidity, TSS and total polyphenol removal. The following CFD operational conditions: 0.48 g/L potassium caseinate, 0.52 g/L bentonite, pH 4.0, temperature 298 K, rapid mix 150 rpm/3 min, slow mix 20 rpm/20 min, sedimentation time 12 h. O_3/Fe^{2+}/UV-C experimental conditions, as follows: pH = 4.0, [Fe^{2+}] = 1.0 mM, ozone flow rate 5 mg/min, air flow 1.0 L/min, agitation 350 rpm, time 600 min, radiation UV-C mercury lamp (254 nm).

Figure 11. Analysis of germination index (GI) regarding the germination of onion, cucumber, lettuce and corn after ozonation (O_3), coagulation–flocculation–decantation (CFD) and combined $O_3 \rightarrow$ CFD

and CFD → O_3 treatments. The following CFD operational conditions were used: 0.48 g/L potassium caseinate, 0.52 g/L bentonite, pH 4.0, temperature 298 K, rapid mix 150 rpm/3 min, slow mix 20 rpm/20 min, sedimentation time 12 h. The following O_3/Fe^{2+}/UV-C experimental conditions were used: pH = 4.0, [Fe^{2+}] = 1.0 mM, ozone flow rate 5 mg/min, air flow 1.0 L/min, agitation 350 rpm, time 600 min, radiation UV-C mercury lamp (254 nm). IG ≤ 50% (high concentration of phytotoxic substances), 80% < IG > 50% (moderated presence of phytotoxic substances), IG ≥ 80% (there are no phytotoxic substances, or they exist in very small dosages).
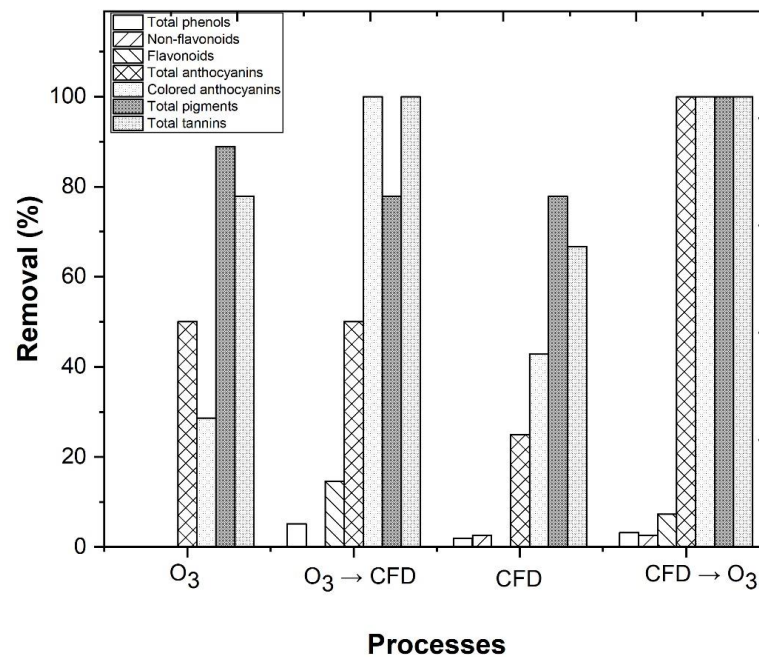
Figure 12. Analysis of total phenols, non-flavonoids, flavonoids, total anthocyanins, colored anthocyanins, total pigments and total tannins removal. The following CFD operational conditions: 0.48 g/L potassium caseinate, 0.52 g/L bentonite, pH 4.0, temperature 298 K, rapid mix 150 rpm/3 min, slow mix 20 rpm/20 min, sedimentation time 12 h. The following O_3/Fe^{2+}/UV-C experimental conditions: pH = 4.0, [Fe^{2+}] = 1.0 mM, ozone flow rate 5 mg/min, air flow 1.0 L/min, agitation 350 rpm, time 600 min and a UV-C mercury lamp (254 nm).

4. Conclusions

In this work, a WW was treated by two different processes, a CFD process, which employed activated sodium bentonite mixed with potassium caseinate, and the advanced oxidation process O_3/Fe^{2+}/UV-C. The combination of both treatment processes in a CFD/O_3/Fe^{2+}/UV-C system, proved to be a feasible method for the treatment of WW, and the main conclusions are summarized as follows:

1. The performance of a CFD process, by application of an SLD statistical design, allows a high removal of turbidity, TSS, TOC, and COD (98.3, 97.6, 44.6, and 48.0%);
2. The application of an ozonation process, under the best operational conditions—pH = 4.0, [Fe^{2+}] = 1.0 mM, ozone flow rate 5 mg/min, air flow 1.0 L/min, agitation 350 rpm, time 600 min, and radiation UV-C mercury lamp (254 nm)—achieves a TOC removal of 63.2%;
3. The O_3/1.0 mM Fe^{2+}/UV-C system is concluded to be very efficient in terms of energy consumption, with an E_{EO} = 1843 kWh m^{-3} order^{-1};
4. The combined processes O_3/CFD and CFD/O_3 achieved high TOC removal (66.1 and 65.5%, respectively). It is also concluded that the performance of the CFD/O_3 process achieves higher biodegradability (0.40);

5. It is concluded that the combined processes O_3/CFD and CFD/O_3 have lower phytotoxicity effects in the germination of plant seeds;

6. The combined process O_3/CFD and CFD/O_3 have the capacity to completely decolor the WW (L* = 100%), through the high removal of phenolic compounds;

7. The combined process O_3/CFD and CFD/O_3 is concluded to decrease the risk of public and environmental health problems.

These results showed that the combination of both treatments was essential to achieve the high degradation of organic matter from the WW. In the future, based on these results, new approaches can be explored, such as optimization of the hydraulic retention time and microbial elimination.

Supplementary Materials: The following are available online at https://www.mdpi.com/article/10.3390/ijerph18168882/s1, Figure S1: Optimization chart. The experimental conditions are as follows: 0.48 g/L potassium caseinate, 0.52 g/L bentonite, pH 4.0, temperature 298 K, rapid mix 150 rpm/3 min, slow mix 20 rpm/20 min, sedimentation time 12 h. X1—potassium caseinate, X2—bentonite, X3—PVPP. Table S1: ANOVA of the regression for turbidity, TSS, COD, and TOC. DF—degrees of freedom; Seq SS—sum of square; Adj SS—sum of adjusted squares; Adj MS—adjusted average squares; F-Value—Fisher ratio. Table S2: Overall results after coagulation–flocculation–decantation process (CFD). The operational conditions are as follows: 0.48 g/L potassium caseinate, 0.52 g/L bentonite, pH 4, temperature 298 K, rapid mix 150 rpm/3 min, slow mix 20 rpm/20 min, sedimentation time 12 h. Table S3: Evaluation of TOC removal through the ozonation process at different pH values (4.0–11). The ozonation experimental conditions are as follows: $[Fe^{2+}]$ = 1.0 mM, ozone flow rate 5 mg/min, air flow 1.0 L/min, agitation 350 rpm, time 600 min, radiation UV-C mercury lamp (254 nm). Table S4: Evaluation of TOC removal through the ozonation process at different Fe^{2+} concentrations (0.5–2.0 mM). The ozonation experimental conditions are as follows: pH = 4.0, ozone flow rate 5 mg/min, air flow 1.0 L/min, agitation 350 rpm, time 600 min, radiation UV-C mercury lamp (254 nm). Table S5: Determination of ozone consumption throughout the ozonation process. The ozonation experimental conditions are as follows: pH = 4.0, $[Fe^{2+}]$ = 1.0 mM, ozone flow rate 5 mg/min, air flow 1.0 L/min, agitation 350 rpm, time 600 min, radiation UV-C mercury lamp (254 nm). Table S6: Overall results after ozonation (O_3), coagulation–flocculation–decantation (CFD), and combined O_3/CFD and CFD/O_3 treatments. The CFD experimental conditions are as follows: 0.48 g/L potassium caseinate, 0.52 g/L bentonite, pH 4, temperature 298 K, rapid mix 150 rpm/3 min, slow mix 20 rpm/20 min, sedimentation time 12 h. The ozonation experimental conditions are as follows: pH 4.0, $[Fe^{2+}]$ = 1.0 mM, ozone flow rate 5 mg/min, air flow 1.0 L/min, agitation 350 rpm, time 600 min, radiation UV-C mercury lamp (254 nm). Table S7: Analysis of seed phytotoxicity after wastewater treatment, by evaluation of germination percentage (G), relative seed germination (RSG), relative root growth (RRG), and germination index (GI). The CFD experimental conditions are as follows: 0.48 g/L potassium caseinate, 0.52 g/L bentonite, pH 4.0, temperature 298 K, rapid mix 150 rpm/3 min, slow mix 20 rpm/20 min, sedimentation time 12 h. The ozonation experimental conditions are as follows: pH 4.0, $[Fe^{2+}]$ = 1.0 mM, ozone flow rate 5 mg/min, air flow 1.0 L/min, agitation 350 rpm, time 600 min, radiation UV-C mercury lamp (254 nm). GI ≤ 50% (high concentration of phytotoxic substances), 80% < GI > 50% (moderated presence of phytotoxic substances), GI ≥ 80% (there are no phytotoxic substances, or they exist in very small dosages). Table S8: Analysis of phenolic composition after ozonation (O_3), coagulation–flocculation–decantation (CFD), and combined O_3/CFD and CFD/O_3 treatments. The CFD experimental conditions are as follows: 0.48 g/L potassium caseinate, 0.52 g/L bentonite, pH 4.0, temperature 298 K, rapid mix 150 rpm/3 min, slow mix 20 rpm/20 min, sedimentation time 12 h. The ozonation experimental conditions are as follows: pH 4.0, $[Fe^{2+}]$ = 1.0 mM, ozone flow rate 5 mg/min, air flow 1.0 L/min, agitation 350 rpm, time 600 min, radiation UV-C mercury lamp (254 nm). Table S9: Analysis of chromatic characteristics (CIELab) after ozonation (O_3), coagulation–flocculation–decantation (CFD), and combined $_{O3}$ → CFD and CFD → O_3 treatments. The CFD experimental conditions are as follows: 0.48 g/L potassium caseinate, 0.52 g/L bentonite, pH 4, temperature 298 K, rapid mix 150 rpm/3 min, slow mix 20 rpm/20 min, sedimentation time 12 h. The ozonation experimental conditions are as follows: pH 4.0, $[Fe^{2+}]$ = 1.0 mM, ozone flow rate 5 mg/min, air flow 1.0 L/min, agitation 350 rpm, time 600 min, radiation UV-C mercury lamp (254 nm).

References

1. OIV-International Organisation of Vine and Wine. *State of the World Vitiviniculture Sector in 2020*; OIV: Paris, France, 2021; pp. 1–19.
2. Ioannou, L.A.; Puma, G.L.; Fatta-Kassinos, D. Treatment of Winery Wastewater by Physicochemical, Biological and Advanced Processes: A Review. *J. Hazard. Mater.* **2015**, *286*, 343–368. [CrossRef] [PubMed]
3. Vlyssides, A.G.; Barampouti, E.M.; Mai, S. Wastewater Characteristics from Greek Wineries and Distilleries. *Water Sci. Technol.* **2005**, *51*, 53–60. [CrossRef]
4. Mosteo, R.; Sarasa, J.; Ormad, M.P.; Ovelleiro, J.L. Sequential Solar Photo-Fenton-Biological System for the Treatment of Winery Wastewaters. *J. Agric. Food Chem.* **2008**, *56*, 7333–7338. [CrossRef] [PubMed]
5. Chatzilazarou, A.; Katsoyannos, E.; Gortzi, O.; Lalas, S.; Paraskevopoulos, Y.; Dourtoglou, E.; Tsaknis, J. Removal of Polyphenols from Wine Sludge Using Cloud Point Extraction. *J. Air Waste Manag. Assoc.* **2010**, *60*, 454–459. [CrossRef] [PubMed]
6. Bolzonella, D.; Zanette, M.; Battistoni, P.; Cecchi, F. Treatment of Winery Wastewater in a Conventional Municipal Activated Sludge Process: Five Years of Experience. *Water Sci. Technol.* **2007**, *56*, 79–87. [CrossRef] [PubMed]
7. Ferreira, R.; Gomes, J.; Martins, R.C.; Costa, R.; Quinta-ferreira, R.M. Winery Wastewater Treatment by Integrating Fenton's Process with Biofiltration by Corbicula Fluminea. *J. Chem. Technol. Biotechnol.* **2018**, *93*, 333–339. [CrossRef]
8. Zhao, C.; Zhou, J.; Yan, Y.; Yang, L.; Xing, G.; Li, H.; Wu, P.; Wang, M.; Zheng, H. Application of Coagulation/Flocculation in Oily Wastewater Treatment: A Review. *Sci. Total Environ.* **2021**, *765*, 142795. [CrossRef] [PubMed]
9. Yang, R.; Li, H.; Huang, M.; Yang, H.; Li, A. A Review on Chitosan-Based Flocculants and Their Applications in Water Treatment. *Water Res.* **2016**, *95*, 59–89. [CrossRef]
10. Braz, R.; Pirra, A.; Lucas, M.S.; Peres, J.A. Combination of Long Term Aerated Storage and Chemical Coagulation/Flocculation to Winery Wastewater Treatment. *Desalination* **2010**, *263*, 226–232. [CrossRef]
11. Amor, C.; De Torres-Socías, E.; Peres, J.; Maldonado, M.I.; Oller, I.; Malato, S.; Lucas, M.S. Mature Landfill Leachate Treatment by Coagulation/Flocculation Combined with Fenton and Solar Photo-Fenton Processes. *J. Hazard. Mater.* **2015**, *286*, 261–268. [CrossRef]
12. Peres, J.A.; De Heredia, J.B.; Dominguez, J.R. Integrated Fenton's Reagent—Coagulation/Flocculation Process for the Treatment of Cork Processing Wastewaters. *J. Hazard. Mater.* **2004**, *107*, 115–121. [CrossRef] [PubMed]
13. Lee, C.S.; Robinson, J.; Chong, M.F. A Review on Application of Flocculants in Wastewater Treatment. *Process Saf. Environ. Prot.* **2014**, *92*, 489–508. [CrossRef]
14. Funai, D.H.; Didier, F.; Giménez, J.; Esplugas, S.; Marco, P.; Machulek, A. Photo-Fenton Treatment of Valproate under UVC, UVA and Simulated Solar Radiation. *J. Hazard. Mater.* **2017**, *323*, 537–549. [CrossRef] [PubMed]
15. Zimbron, J.A.; Reardon, K.F. Fenton's Oxidation of Pentachlorophenol. *Water Res.* **2009**, *43*, 1831–1840. [CrossRef] [PubMed]
16. Lucas, M.S.; Mouta, M.; Pirra, A.; Peres, J.A. Winery Wastewater Treatment by a Combined Process: Long Term Aerated Storage and Fenton's Reagent. *Water Sci. Technol.* **2009**, *60*, 1089–1095. [CrossRef] [PubMed]

17. Lucas, M.S.; Mosteo, R.; Maldonado, M.I.; Malato, S.; Peres, J.A. Solar Photochemical Treatment of Winery Wastewater in a CPC Reactor. *J. Agric. Food Chem.* **2009**, *57*, 11242–11248. [CrossRef] [PubMed]

18. Lucas, M.S.; Dias, A.A.; Bezerra, R.M.; Peres, J.A. Gallic Acid Photochemical Oxidation as a Model Compound of Winery Wastewaters. *J. Environ. Sci. Health Part A* **2008**, *43*, 1288–1295. [CrossRef]

19. Rodríguez-Chueca, J.; Amor, C.; Silva, T.; Dionysiou, D.D.; Li Puma, G.; Lucas, M.S.; Peres, J.A. Treatment of Winery Wastewater by Sulphate Radicals: HSO5-/Transition Metal/UV-A LEDs. *Chem. Eng. J.* **2017**, *310*, 473–483. [CrossRef]

20. Rodríguez-Chueca, J.; Amor, C.; Mota, J.; Lucas, M.S.; Peres, J.A. Oxidation of Winery Wastewater by Sulphate Radicals: Catalytic and Solar Photocatalytic Activations. *Environ. Sci. Pollut. Res.* **2017**, *24*, 22414–22426. [CrossRef]

21. Jorge, N.; Teixeira, A.R.; Lucas, M.S.; Peres, J.A. Combination of Adsorption in Natural Clays and Photo-Catalytic Processes for Winery Wastewater Treatment. In *Advances in Geoethics and Groundwater Management: Theory and Practice for a Sustainable Development*; Abrunhosa, M., Chambel, A., Peppoloni, S., Chaminé, H.I., Eds.; Springer: Cham, Switzerland, 2021; pp. 291–294. ISBN 978-3-030-59320-9.

22. Guimarães, V.; Teixeira, A.R.; Lucas, M.S.; Peres, J.A. Effect of Zr Impregnation on Clay-Based Materials for H_2O_2-Assisted Photocatalytic Wet Oxidation of Winery Wastewater. *Water* **2020**, *12*, 3387. [CrossRef]

23. Lucas, M.S.; Peres, J.A.; Li Puma, G. Treatment of Winery Wastewater by Ozone-Based Advanced Oxidation Processes (O_3, O_3/UV and O_3/UV/H_2O_2) in a Pilot-Scale Bubble Column Reactor and Process Economics. *Sep. Purif. Technol.* **2010**, *72*, 235–241. [CrossRef]

24. Wang, J.; Chen, H. Catalytic Ozonation for Water and Wastewater Treatment: Recent Advances and Perspective. *Sci. Total Environ.* **2020**, *704*, 135249. [CrossRef]

25. Liu, Z.; Demeestere, K.; Hulle, S. Van Comparison and Performance Assessment of Ozone-Based AOPs in View of Trace Organic Contaminants Abatement in Water and Wastewater: A Review. *J. Environ. Chem. Eng.* **2021**, *9*, 105599. [CrossRef]

26. Yao, W.; Waqi, S.; Rehman, U.; Wang, H.; Yang, H.; Yu, G.; Wang, Y. Pilot-Scale Evaluation of Micropollutant Abatements by Conventional Ozonation, UV/O3, and an Electro-Peroxone Process. *Water Res.* **2018**, *138*, 106–117. [CrossRef]

27. Lan, B.Y.; Nigmatullin, R.; Li Puma, G. Ozonation Kinetics of Cork-Processing Water in a Bubble Column Reactor. *Water Res.* **2008**, *42*, 2473–2482. [CrossRef]

28. Monteagudo, J.M.; Carmona, M.; Dura, A. Photo-Fenton-Assisted Ozonation of p-Coumaric Acid in Aqueous Solution. *Chemosphere* **2005**, *60*, 1103–1110. [CrossRef] [PubMed]

29. Benitez, F.J.; Real, F.J.; Acero, J.L.; Garcia, J.; Sanchez, M. Kinetics of the Ozonation and Aerobic Biodegradation of Wine Vinasses in Discontinuous and Continuous Processes. *J. Hazard. Mater.* **2003**, *101*, 203–218. [CrossRef]

30. *Standard Methods for the Examination of Water and Wastewater*, 20th ed; American Public Health Association, American Water Works Association; Water Environment Federation: Washington, DC, USA, 1999.

31. Singleton, V.L.; Rossi, J.A. Colorimetry of Total Phenolics with Phosphomolybdic-Phosphotungstic Acid Reagents. *Am. J. Enol. Vitic.* **1965**, *16*, 144–158.

32. OECD. *OECD Guidelines for the Testing of Chemicals*; Terrestrial Plant Test: Paris, France, 2004; Volume 208.

33. Varnero, M.T.; Rojas, C.; Orellana, R. Índices de Fitotoxicidad En Residuos Orgánicos Durante El Compostaje. *Rev. Cienc. Suelo Y Nutr. Veg.* **2007**, *7*, 28–37. [CrossRef]

34. Tiquia, S.M.; Tam, N.F.Y. Elimination of Phytotoxicity during Co-Composting of Spent Pig-Manure Sawdust Litter and Pig Sludge. *Bioresour. Technol.* **1998**, *65*, 43–49. [CrossRef]

35. OIV. *Compendium of International Methods of Wine and Must Analysis—Volume I*, 2017th ed.; OIV: Paris, France, 2017; ISBN 979-10-91799-64-5.

36. Curvelo-Garcia, A. Controlo de qualidade dos vinhos. In *Química Enológica e Métodos Analíticos. Avanços Recentes no Controlo da Qualidade de Vinhos e de Outros Produtos Vitivinícolas*; António Sérgio Curvelo Garcia e Paulo Barros, Ed.; Engebook/Publindustria; Edições Técnicas, Lda: Porto, Portugal, 1988; ISBN 978-989-723-118-6.

37. Kramling, T.E.; Singleton, V.L. An Estimate of the Nonflavonoid Phenols in Wines. *Am. J. Enol. Vitic.* **1969**, *20*, 86–92.

38. Ribéreau-Gayon, P.; Glories, Y.; Maujean, A.; Dubourdieu, D. *Handbook of Enology Volume 2 The Chemistry of Wine Stabilization and Treatments*, 2nd ed.; John Wiley & Sons Inc.: Chichester, UK, 2006; Volume 2, ISBN 9780470010396.

39. Somers, T.C.; Evans, M.E. Spectral Evaluation of Young Red Wines: Anthocyanin Equilibria, Total Phenolics, Free and Molecular SO_2, "Chemical Age". *J. Sci. Food Agric.* **1977**, *28*, 279–287. [CrossRef]

40. Ribéreau-Gayon, P.; Stonestreet, E. Dosage Des Tanins Du Vin Rouge et Détermination de Leur Structure. *Chim. Anal.* **1966**, *48*, 188.

41. Spagna, G.; Pifferi, G.; Rangoni, C.; Mattivi, F.; Nicolinib, G.; Palmonari, R. The Stabilization of White Wines by Adsorption of Phenolic Compounds on Chitin and Chitosan. *Food Res. Int.* **1996**, *29*, 241–248. [CrossRef]

42. Schanda, J. *Colorimetry: Understanding the CIE System*; John Wiley & Sons, Inc.: Hoboken, NJ, USA, 2007; ISBN 978-0-470-04904-4.

43. Xue, J.; Wang, T.; Hu, Q.; Zhou, M.; Luo, Y. A Novel and Organic Solvent-Free Preparation of Solid Lipid Nanoparticles Using Natural Biopolymers as Emulsi Fi Er and Stabilizer. *Int. J. Pharm.* **2017**, *531*, 59–66. [CrossRef]

44. Ren, J.; Hou, Y.; Fan, G.; Zhang, L.; Li, X.; Yin, K.; Pan, S. Extraction of Orange Pectin Based on the Interaction between Sodium Caseinate and Pectin. *Food Chem.* **2019**, *283*, 265–274. [CrossRef] [PubMed]

45. Borodko, Y.; Habas, S.E.; Koebel, M.; Yang, P.; Frei, H.; Somorjai, G.A. Probing the Interaction of Poly (Vinylpyrrolidone) with Platinum Nanocrystals by UV—Raman and FTIR. *J. Phys. Chem. B* **2006**, *110*, 23052–23059. [CrossRef]

Int. J. Environ. Res. Public Health **2021**, *18*, 8882

24 of 26

46. Abdelghany, A.M.; Mekhail, M.S.; Abdelrazek, E.M.; Aboud, M.M. Combined DFT/FTIR Structural Studies of Monodispersed PVP/Gold and Silver Nano Particles. *J. Alloys Compd.* **2015**, *646*, 326–332. [CrossRef]

47. Laot, C.M.; Marand, E.; Oyama, H.T. Spectroscopic Characterization of Molecular Interdiffusion at a Poly (Vinylpyrrolidone)/Vinyl Ester Interface. *Polymer* **1999**, *40*, 1095–1108. [CrossRef]

48. Lewandowska, K. The Miscibility of Poly (Vinyl Alcohol)/Poly (N-Vinylpyrrolidone) Blends Investigated in Dilute Solutions and Solids. *Eur. Polym. J.* **2005**, *41*, 55–64. [CrossRef]

49. Abdelaziz, M.; Abdelrazek, E.M. Effect of Dopant Mixture on Structural, Optical and Electron Spin Resonance Properties of Polyvinyl Alcohol. *Phys. B Condens. Matter* **2007**, *390*, 1–9. [CrossRef]

50. Abdelrazek, E.M.; Elashmawi, I.S.; El-khodary, A.; Yassin, A. Structural, Optical, Thermal and Electrical Studies on PVA/PVP Blends Filled with Lithium Bromide. *Curr. Appl. Phys.* **2010**, *10*, 607–613. [CrossRef]

51. Tawansi, A.; El-Khodary, A.; Abdelnaby, M.M. A Study of the Physical Properties of FeCl3 Filled PVA. *Curr. Appl. Phys.* **2005**, *5*, 572–578. [CrossRef]

52. Schuttlefield, J.D.; Cox, D.; Grassian, V.H. An Investigation of Water Uptake on Clays Minerals Using ATR-FTIR Spectroscopy Coupled with Quartz Crystal Microbalance Measurements. *J. Geophys. Res. Atmos.* **2007**, *112*, D21. [CrossRef]

53. Sevim, A.M.; Hojiyev, R.; Gül, A.; Celik, M.S. Preparation of Novel Heterogeneous Catalysts by Adsorption of a Cationic Tetrapyrrole on to Bentonite: Equilibrium, Kinetics, and Thermodynamics. *Mon. Für Chem. Chem. Mon.* **2012**, *143*, 385–400. [CrossRef]

54. Żymankowska-kumon, S.; Holtzer, M.; Olejnik, E.; Bobrowski, A. Influence of the Changes of the Structure of Foundry Bentonites on Their Binding Properties. *Mater. Sci.* **2012**, *18*, 57–61. [CrossRef]

55. Hojiyev, R.; Ulcay, Y.; Çelik, M.S. Development of a Clay-Polymer Compatibility Approach for Nanocomposite Applications. *Appl. Clay Sci.* **2017**, *146*, 548–556. [CrossRef]

56. Guimarães, V.; Teixeira, A.R.; Lucas, M.S.; Silva, A.M.T.; Peres, J.A. Pillared Interlayered Natural Clays as Heterogeneous Photocatalysts for H2O2-Assisted Treatment of a Winery Wastewater. *Sep. Purif. Technol.* **2019**, *228*, 115768. [CrossRef]

57. Thommes, M.; Kaneko, K.; Neimark, A.V.; Olivier, J.P.; Rodriguez-Reinoso, F.; Rouquerol, J.; Sing, K.S. Physisorption of Gases, with Special Reference to the Evaluation of Surface Area and Pore Size Distribution (IUPAC Technical Report). *Pure Appl. Chem.* **2015**, *87*, 1051–1069. [CrossRef]

58. Anderson, M.J. A New Method for Non-Parametric Multivariate Analysis of Variance. *Austral Ecol.* **2001**, *26*, 32–46. [CrossRef]

59. Bahadir, K.K.; Rauf, M.A. Application of Response Surface Analysis to the Photolytic Degradation of Basic Red 2 Dye. *Chem. Eng. J.* **2008**, *138*, 166–171. [CrossRef]

60. Joglekar, A.M.; May, A.T. Product Excellence through Design of Experiments. *Cereal Foods World* **1987**, *32*, 857–868.

61. Muhamad, M.H.; Mohamad, S.R.S.A.A.B.; Rahman, R.A.; Kadhum, A.A.H. Application of Response Surface Methodology (RSM) for Optimisation of COD, NH3 e N and 2, 4-DCP Removal from Recycled Paper Wastewater in a Pilot-Scale Granular Activated Carbon Sequencing Batch Bio Fi Lm Reactor (GAC-SBBR). *J. Environ. Manag.* **2013**, *121*, 179–190. [CrossRef] [PubMed]

62. Ahmad, A.L.; Wong, S.S.; Teng, T.T.; Zuhairi, A. Optimization of Coagulation—Flocculation Process for Pulp and Paper Mill Effluent by Response Surface Methodological Analysis. *J. Hazard. Mater.* **2007**, *145*, 162–168. [CrossRef]

63. Chantarangsi, W.; Liu, W.; Bretz, F.; Kiatsupaibul, S.; Hayter, A.J. Computation Normal Probability Plots with Confidence for the Residuals in Linear Regression. *Commun. Stat. Comput.* **2018**, *47*, 367–379. [CrossRef]

64. Harbi, B.; Chaieb, K.; Mahdouani, K.; Bakhrouf, A. PCR Detection of Nitrite Reductase Genes (NirK and NirS) and Use of Active Consortia of Constructed Ternary Adherent Staphylococcal Cultures via Mixture Design for a Denitrification Process. *World J. Microbiol. Biotechnol.* **2010**, *26*, 473–480. [CrossRef]

65. Cosme, F.; Ricardo-da-Silva, J.M.; Laureano, O. Interactions between Protein Fining Agents and Proanthocyanidins in White Wine. *Food Chem.* **2008**, *106*, 536–544. [CrossRef]

66. Cosme, F.; Capão, I.; Filipe-Ribeiro, L.; Bennett, R.N.; Mendes-Faia, A. Evaluating Potential Alternatives to Potassium Caseinate for White Wine Fining: Effects on Physicochemical and Sensory Characteristics. *Food Sci. Technol.* **2012**, *46*, 382–387. [CrossRef]

67. Cosme, F.; Ricardo-Da-Silva, J.M.; Laureano, O. Protein Fining Agents: Characterization and Red Wine Fining Assays. *Ital. J. Food Sci.* **2007**, *19*, 39–56.

68. Benna, M.; Magnin, A.; Bergaya, F. Effect of PH on Rheological Properties of Purified Sodium Bentonite Suspensions. *J. Colloid Interface Sci.* **1999**, *218*, 442–455. [CrossRef]

69. Guimarães, V.; Lucas, M.S.; Peres, J.A. Combination of Adsorption and Heterogeneous Photo-Fenton Processes for the Treatment of Winery Wastewater. *Environ. Sci. Pollut. Res.* **2019**, *26*, 31000–31013. [CrossRef]

70. Guimarães, V.; Rodríguez-castellón, E.; Algarra, M.; Rocha, F.; Bobos, I. Influence of PH, Layer Charge Location and Crystal Thickness Distribution on U(VI) Sorption onto Heterogeneous Dioctahedral Smectite. *J. Hazard. Mater.* **2016**, *317*, 246–258. [CrossRef]

71. Laborde, B.; Moine-Ledoux, V.; Richard, T.; Saucier, C.; Dubourdieu, D.; Monti, J.-P. PVPP−Polyphenol Complexes: A Molecular Approach. *J. Agric. Food Chem.* **2006**, *54*, 4383–4389. [CrossRef]

72. Pierpoint, W.S. The Extraction of Enzymes from Plant Tissues Rich in Phenolic Compounds. *Protein Purif. Protoc.* **1996**, *59*, 69–80. [CrossRef]

73. Howe, K.J.; Hand, D.W.; Crittenden, J.C.; Trussell, R.R.; Tchobanoglous, G. *Principles of Water Treatment*; John Wiley & Sons, Inc.: Hoboken, NJ, USA, 2012; ISBN 9780470405383.

74. Braga, A.; Cosme, F.; Ricardo-da-Silva, J.M.; Laureano, O. Gelatine, Casein and Potassium Caseinate as Distinct Wine Fining Agents: Different Effects on Colour, Phenolic Compounds and Sensory Characteristics. *OENO One* **2007**, *41*, 203–214. [CrossRef]
75. Hunter, R.J. *Foundations of Colloid Science*, 2nd ed.; Oxford University Press: Oxford, UK, 2001; ISBN 978-0-19-850502-0.
76. Huang, Y.; Jiang, J.; Ma, L.; Wang, Y.; Liang, M.; Zhang, Z.; Li, L. Iron Foam Combined Ozonation for Enhanced Treatment of Pharmaceutical Wastewater. *Environ. Res.* **2020**, *183*, 109205. [CrossRef] [PubMed]
77. Hassanshahi, N.; Karimi-jashni, A. Comparison of Photo-Fenton, $O_3/H_2O_2/UV$ and Photocatalytic Processes for the Treatment of Gray Water. *Ecotoxicol. Environ. Saf.* **2018**, *161*, 683–690. [CrossRef] [PubMed]
78. Hoigne, J.; Bader, H. The Role of Hydroxyl Radical Reactions in Ozonation Processes in Aqueous Solutions. *Water Res.* **1976**, *10*, 377–386. [CrossRef]
79. Agustina, T.E.; Ang, H.M.; Vareek, V.K. A Review of Synergistic Effect of Photocatalysis and Ozonation on Wastewater Treatment. *J. Photochem. Photobiol. C Photochem. Rev.* **2005**, *6*, 264–273. [CrossRef]
80. Hodges, J.T.; Viallon, J.; Brewer, P.J.; Drouin, B.J.; Gorshelev, V.; Janssen, C.; Lee, S.; Possolo, A.; Smith, M.A.H.; Walden, J.; et al. Recommendation of a Consensus Value of the Ozone Absorption Cross-Section at 253.65 Nm Based on a Literature Review. *Metrologia* **2019**, *56*, 034001. [CrossRef]
81. Jodpimai, S.; Boonduang, S.; Limsuwan, P. Sensors and Actuators B: Chemical Inline Ozone Concentration Measurement by a Visible Absorption Method at Wavelength 605 Nm. *Sens. Actuators B. Chem.* **2016**, *222*, 8–14. [CrossRef]
82. Piera, E.; Calpe, J.C.; Brillas, E.; Domènech, X.; Peral, J. 2,4-Dichlorophenoxyacetic Acid Degradation by Catalyzed Ozonation: $TiO_2/UVA/O_3$ and Fe (II)/UVA/O_3 Systems. *Appl. Catal. B Environ.* **2000**, *27*, 169–177. [CrossRef]
83. Adar, E. Optimization of Triple Dye Mixture Removal by Oxidation with Fenton. *Int. J. Environ. Sci. Technol.* **2020**, *17*, 4431–4440. [CrossRef]
84. Chaturvedi, N.K.; Katoch, S.S. O-Anisidine Degradation by Fenton's Reagent and Reaction Time Estimation. *Pollution* **2020**, *6*, 127–134. [CrossRef]
85. Clarizia, L.; Russo, D.; Di Somma, I.; Marotta, R.; Andreozzi, R. Homogeneous Photo-Fenton Processes at near Neutral PH: A Review. *Appl. Catal. B Environ.* **2017**, *209*, 358–371. [CrossRef]
86. Dowd, K.O.; Pillai, S.C. Photo-Fenton Disinfection at near Neutral PH: Process, Parameter Optimization and Recent Advances. *J. Environ. Chem. Eng.* **2020**, *8*, 104063. [CrossRef]
87. Chang, R. *CHEMISTRY*, 10th ed.; The McGraw-Hill Companies, Inc.: New York, NY, USA, 2010; ISBN 978–0–07–351109–2.
88. Ebrahiem, E.E.; Al-Maghrabi, M.N.; Mobarki, A.R. Removal of Organic Pollutants from Industrial Wastewater by Applying Photo-Fenton Oxidation Technology. *Arab. J. Chem.* **2017**, *10*, S1674–S1679. [CrossRef]
89. Quiroz, A.C.; Barrera-díaz, C.; Roa-morales, G.; Hern, P.B.; Romero, R.; Natividad, R. Wastewater Ozonation Catalyzed by Iron. *Ind. Eng. Chem. Res.* **2011**, *50*, 2488–2494. [CrossRef]
90. Bolton, J.R.; Bircher, K.G.; Tumas, W.; Tolman, C.A. Figures-of-Merit for the Technical Development and Application of Advanced Oxidation Technologies for Both Electric-and Solar-Driven Systems (IUPAC Technical Report). *Pure Appl. Chem.* **2001**, *73*, 627–637. [CrossRef]
91. Bessegato, G.G.; De Souza, J.C.; Cardoso, J.C.; Zanoni, M.V.B. Assessment of Several Advanced Oxidation Processes Applied in the Treatment of Environmental Concern Constituents from a Real Hair Dye Wastewater. *J. Environ. Chem. Eng.* **2018**, *6*, 2794–2802. [CrossRef]
92. Cardoso, J.C.; Bessegato, G.G.; Zanoni, M.V.B. Efficiency Comparison of Ozonation, Photolysis, Photocatalysis and Photoelectro-catalysis Methods in Real Textile Wastewater Decolorization. *Water Res.* **2016**, *98*, 39–46. [CrossRef] [PubMed]
93. Kang, W.; Chen, S.; Yu, H.; Xu, T.; Wu, S.; Wang, X.; Lu, N.; Quan, X.; Liang, H. Photocatalytic Ozonation of Organic Pollutants in Wastewater Using a Flowing through Reactor. *J. Hazard. Mater.* **2021**, *405*, 124277. [CrossRef] [PubMed]
94. Liu, S.; Wang, Q.; Zhai, X.; Huang, Q.; Huang, P. Improved Pretreatment (Coagulation-Floatation and Ozonation) of Younger Landfill Leachate by Microbubbles. *Water Environ. Res.* **2010**, *82*, 657–665. [CrossRef] [PubMed]
95. Bu, F.; Gao, B.; Shen, X.; Wang, W.; Yue, Q. The Combination of Coagulation and Ozonation as a Pre-Treatment of Ultrafiltration in Water Treatment. *Chemosphere* **2019**, *231*, 349–356. [CrossRef] [PubMed]
96. Casa, R.; D'Annibale, A.; Pieruccetti, F.; Stazi, S.; Sermanni, G.G.; Cascio, B.L. Reduction of the Phenolic Components in Olive-Mill Wastewater by an Enzymatic Treatment and Its Impact on Durum Wheat (Triticum Durum Desf.) Germinability. *Chemosphere* **2003**, *50*, 959–966. [CrossRef]
97. Komilis, D.P.; Karatzas, E.; Halvadakis, C.P. The Effect of Olive Mill Wastewater on Seed Germination after Various Pretreatment Techniques. *J. Environ. Manag.* **2005**, *74*, 339–348. [CrossRef]
98. Saadi, I.; Laor, Y.; Raviv, M.; Medina, S. Land Spreading of Olive Mill Wastewater: Effects on Soil Microbial Activity and Potential Phytotoxicity. *Chemosphere* **2007**, *66*, 75–83. [CrossRef]
99. Mosse, K.P.M.; Patti, A.F.; Christen, E.W.; Cavagnaro, T.R. Winery Wastewater Inhibits Seed Germination and Vegetative Growth of Common Crop Species. *J. Hazard. Mater.* **2010**, *180*, 63–70. [CrossRef]

Int. J. Environ. Res. Public Health **2021**, *18*, 8882

26 of 26

100. Milheiro, J.; Filipe-Ribeiro, L.; Cosme, F.; Nunes, F.M. A Simple, Cheap and Reliable Method for Control of 4-Ethylphenol and 4-Ethylguaiacol in Red Wines. Screening of Fining Agents for Reducing Volatile Phenols Levels in Red Wines. *J. Chromatogr. B* **2017**, *1041–1042*, 183–190. [CrossRef]

101. Filipe-Ribeiro, L.; Milheiro, J.; Matos, C.C.; Cosme, F.; Nunes, F.M. Data on Changes in Red Wine Phenolic Compounds, Headspace Aroma Compounds and Sensory Profile after Treatment of Red Wines with Activated Carbons with Different Physicochemical Characteristics. *Data Br.* **2017**, *12*, 188–202. [CrossRef]